Nano Research
DOI 10.1007/s12274-017-1596-1
Review Article
ISSN 1998-0124
CN 11-5974/O4

Nanoscale perspective: Materials designs and understandings in lithium metal anodes

Dingchang Lin[1], Yayuan Liu[1], Allen Pei[1], and Yi Cui[1,2] (✉)

[1] *Department of Materials Science and Engineering, Stanford University, Stanford, California 94305, USA*
[2] *Stanford Institute for Materials and Energy Sciences, SLAC National Accelerator Laboratory, 2575 Sand Hill Road, Menlo Park, California 94025, USA*

Received: 13 February 2017
Revised: 12 March 2017
Accepted: 14 March 2017

KEYWORDS
lithium metal anodes, nanoscale lithium nucleation

ABSTRACT

Li metal chemistry is a promising alternative with a much higher energy density than that of state-of-the-art Li-ion counterparts. However, significant challenges including safety issues and poor cyclability have severely impeded Li metal technology from becoming viable. In recent years, nanotechnologies have become increasingly important in materials design and fabrication for Li metal anodes, contributing to major progress in the field. In this review, we first introduce the main achievements in Li metal battery systems fulfilled by nanotechnologies, particularly regarding Li metal anode design and protection, ultrastrong separator engineering, safety monitoring, and smart functions. Next, we introduce recent studies on nanoscale Li nucleation/deposition. Finally, we discuss possible future research directions. We hope this review delivers an overall picture of the role of nanoscale approaches in the recent progress of Li metal battery technology and inspires more research in the future.

1 Introduction

Li metal is a promising anode candidate for next-generation Li-based batteries [1–4]. As an alternative to traditional carbonaceous anodes, Li metal exhibits a theoretical capacity greater by one order of magnitude at 3,860 mA·h·g^{-1}, with the lowest standard electrochemical potential of −3.04 V vs. a standard hydrogen electrode (SHE). Together, these properties guarantee that Li metal provides the highest energy density among all anode alternatives in a full cell [5–8].

The development of Li metal anodes for Li secondary cells began in the early 1970s, when Whittingham et al. developed the first Li metal-based secondary cell at Exxon [1]. However, the widespread commercialization of Li metal anodes remains stagnant today, mainly because of notorious safety hazards and poor cyclability [9, 10]. In the meantime, carbonaceous anodes have been successfully developed that promptly took the place of Li metal. Li-free anodes are well matched with Li-containing discharged cathode materials such as $LiCoO_2$ and $LiFePO_4$. The stable solid electrolyte interphase (SEI) guarantees minimal side reactions and a wide voltage window of 4 V or more. This

Address correspondence to yicui@stanford.edu

Li-ion chemistry exhibits fairly stable cycling and a much higher energy density than Ni–H systems, permitting great success in various civilian applications. Despite these breakthroughs, Li-ion chemistry has the major drawback of insufficient energy density, particularly in the context of increasing demand for light-weight, high-energy, and more portable energy storage devices. The energy density of conventional Li-ion systems remains far below that which can be reached by a Li metal battery system, because of the high weight proportion of host materials on both the cathode and anode sides. As a consequence, developing Li metal-based systems (e.g., Li–air and Li–S systems) with much higher energy densities has become very attractive [11].

The major problems of Li metal, such as exaggerated dendritic growth and severe side reactions, originate at the nanoscale [3, 4, 12, 13]. The interfacial stability between the electrolyte and Li is critical, depending on the SEI of only a few nanometers in thickness [14–16]. Because of the high reactivity and infinite relative volume change of Li during cycling, the thin and heterogenous SEI is vulnerable to fracture, exposing highly reactive fresh Li with concentrated Li-ion flux [4, 17, 18]. Under this circumstance, nanoscale examinations and approaches to materials design are of great importance. Recently, nanoscale approaches have created new possibilities in developing stable Li anodes, while the nanoscale investigation of Li nucleation and deposition has offered important fundamental insights.

In this contribution, we first summarize the recent key progress in Li anode design enabled by nanoscale approaches, and then introduce the current understanding of Li metal nucleation and deposition at the nanoscale. This review outlines the new opportunities created by nanotechnology in Li anode design, highlights the importance of nanoscale perspectives, and offers possible insights to future innovation in this field.

2 Design of artificial SEI

The interfacial stability is critical in Li metal research. Without stable interfacial passivation, the prevention of Li corrosion and the formation of stable Li anodes are unlikely. However, in most conditions using liquid electrolytes, it is difficult to attain an SEI with sufficient stability. As a consequence, the development of stable artificial SEIs has become important. In principle, the concept of an artificial SEI involves the fabrication of a more stable interfacial layer on the Li metal before battery assembly; this layer should have more controllable chemistry or advanced nanotechnologies. A common strategy to fabricate artificial SEIs is to exploit more controllable chemistries that can react *in-situ* with Li, thereby replacing the conventional SEI formation process in electrochemical cells. Such pre-engineered interfacial layers can not only better protect the Li metal from electrolyte corrosion and enhance the cycling stability, but also improve the processability of Li metal in air. In this section, we summarize some recent progress in the design and fabrication of artificial SEIs.

Adding inorganic surface passivation layers to Li metal is the most common strategy to generate artificial SEIs. For example, LiF [19–21], Al_2O_3 [22–25], Li_3N [26, 27], Li_3PO_4 [28, 29], and Li phosphorus oxynitride (LiPON) [30] have been explored extensively as surface protections. Atomic layer deposition (ALD) is useful for fabricating artificial SEIs because it permits high uniformity [24, 25, 31]. Noked et al. utilized ALD to coat Li metal with Al_2O_3, which can be spontaneously converted to the Li-ion conductive $Li_xAl_2O_3$ phase by reacting with Li (Fig. 1(a)) [24]. A thin coating of 14 nm has been proven to effectively prevent air corrosion; the metal maintains a silvery color even in ambient air with the relative humidity (RH) of 40% (Fig. 1(b), right), whereas unprotected Li instantly turns black under equal conditions (Fig. 1(b), left). In contrast to the vapor deposition of ALD, Guo et al. developed an *in situ* reaction of Li metal with liquid polyphosphoric acid to form an artificial Li_3PO_4 SEI, which also exhibited Li-ion conductivity (Fig. 1(c)) [28]. After 200 galvanostatic cycles (0.5 C, ~0.5 $mA{\cdot}h{\cdot}cm^{-2}$), the untreated Li metal electrode was observed to accumulate a thick porous surface layer of ~200 μm in thickness (Fig. 1(d)), while the treated electrode showed a relatively thin surface layer (Fig. 1(e)).

Other than inorganic artificial SEIs, polymeric coatings are of great interest because they offer good flexibility or even elasticity [32–35]. For the SEI layer,

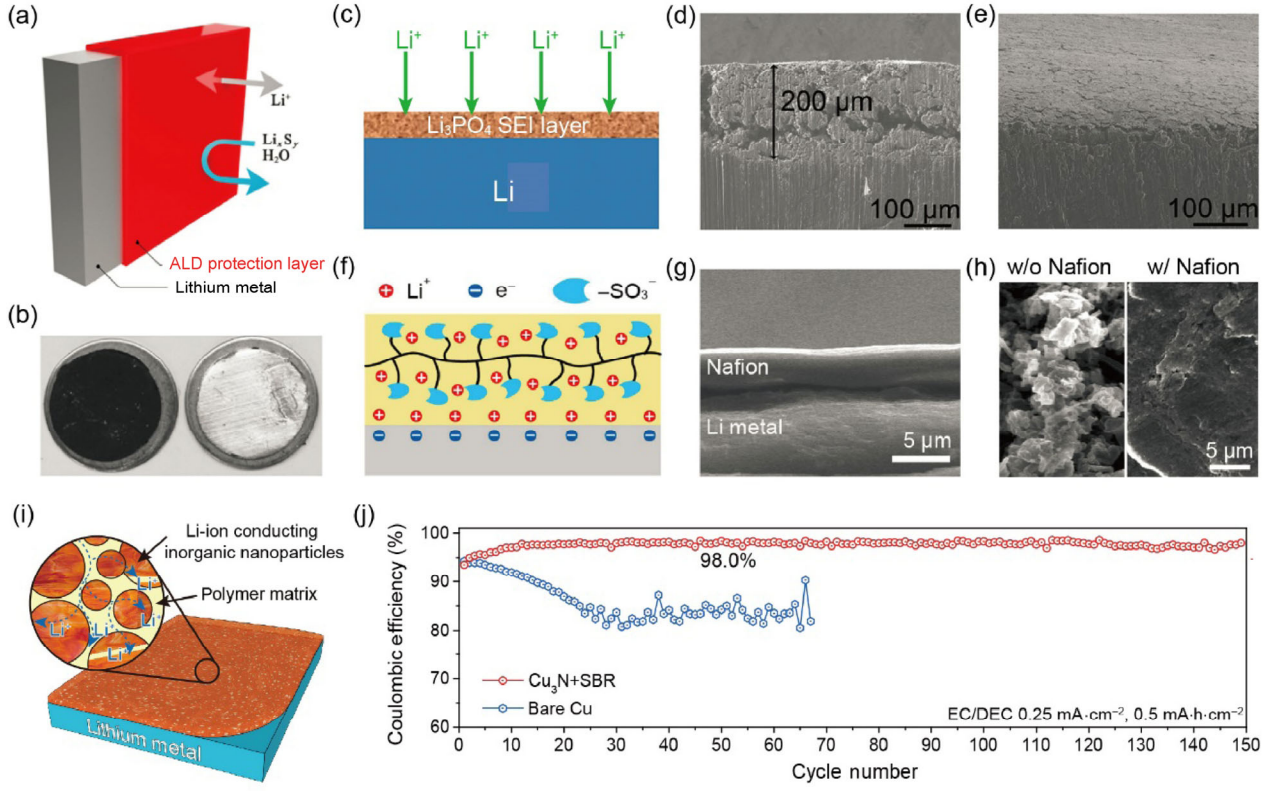

Figure 1 (a) ALD of Al_2O_3 on the surface of Li foil, preventing corrosion by Li polysulfides and H_2O (reproduced with the permission from [24], © American Chemical Society 2015). (b) Comparison of 14-h air exposure (40% RH, 25 °C) of Li foil without (left) and with (right) ALD Al_2O_3. Li without Al_2O_3 coating is corroded, turning black, while that with Al_2O_3 maintains a silvery color (reproduced with the permission from [24], © American Chemical Society 2015). (c) Schematic showing the Li_3PO_4 artificial SEI coating on Li foil (reproduced with the permission from [28], © WILEY-VCH Verlag GmbH & Co. KGaA, Weinheim 2016). (d) and (e) Side-view SEM images of Li foil (d) and Li_3PO_4-coated Li (e) after 200 cycles, where the bare Li foil exhibits a thick porous structure on the top (reproduced with the permission from [28], © WILEY-VCH Verlag GmbH & Co. KGaA, Weinheim 2016). (f) and (g) Schematic of Nafion-coated Li foil (f) and corresponding cross-sectional SEM image (g) (reproduced with the permission from [36], © Nature Publishing Group 2015). (h) Comparison of Li metal electrode surfaces without (left) and with (right) Nafion coating after 100 cycles (reproduced with the permission from [36], © Nature Publishing Group 2015). (i) Schematic of Li_3N nanoparticles embedded in SBR polymer matrix as a hybrid artificial SEI with good flexibility and Li-ion conductivity (reproduced with the permission from [39], © WILEY-VCH Verlag GmbH & Co. KGaA, Weinheim 2017). (j) CE stability of the Li_3N–SBR-coated Cu foil at a current density of 0.25 mA·cm^{-2} (0.5 mA·h·cm^{-2}), where the Li_3N–SBR-coated Cu foil exhibited much more stable cyclability with the high CE of 98.0% (reproduced with the permission from [39], © WILEY-VCH Verlag GmbH & Co. KGaA, Weinheim 2017).

a certain level of flexibility is preferential, in order to accommodate dramatic surface fluctuations during cycling. For the cycling of a practical areal amount of Li (>3 mA·h·cm^{-2}), the surface fluctuation of Li metal can reach tens of micrometers. A thin inorganic layer is unlikely to accommodate this fluctuation without cracking. With this consideration, Kim et al. developed a Li–Nafion coating on a Li metal surface as an artificial SEI (Fig. 1(f)); Nafion exhibits high ionic conductivity as well as single-ion conduction [36]. The scanning electron microscopy (SEM) image in Fig. 1(g) shows that the Nafion layer coating is uniform with a thickness of a few micrometers. Figure 1(h) shows the surface morphologies of the uncoated Li metal (left) and Nafion-coated Li metal (right) after 100 cycles (~1.5 mA·h·cm^{-2}). The surface of the uncoated Li exhibits a porous morphology with dendrites, while the Nafion-coated counterpart retains relatively flat and dense Li. Similar effects were also observed independently by other research groups using either thin Nafion coatings or Nafion electrolytes [37, 38].

In addition to purely inorganic or polymeric artificial

SEIs, composites of ceramics and polymers have attracted growing attention recently. Composites can combine good flexibility and high mechanical strength in artificial SEIs. Recently, Cui et al. demonstrated a composite of Cu_3N nanoparticles and styrene butadiene rubber (SBR) [39]. In a cell environment, the embedded Cu_3N nanoparticles can be spontaneously converted to Li-ion conductive Li_3N nanoparticles (Fig. 1(i)), which serve a two-fold purpose as both strong physical barriers and Li-ion conducting media. The as-obtained composite exhibits not only a high modulus of ~0.8 GPa, but also excellent flexibility. The film on Cu shows the high Coulombic efficiency (CE) of ~98% for at least 150 cycles, outperforming the unmodified Cu foil (Fig. 1(j)). A similar blend of polymers with inorganic materials was also demonstrated in other systems, such as a poly(3,4-ethylenedioxythiophene)–polyethylene glycol (PEDOT–PEG)/AlF_3 composite [40].

Moreover, approaches that mimic the formation of good "real" SEIs are also of great interest. Previously, it was found that the SEI formed in the presence of Li polysulfide and $LiNO_3$ effectively suppressed Li dendrite growth and improved cycle life [41]. Zhang et al. developed an *ex-situ* electrochemical method to engineer a stable SEI in a 1-M Li bistrifluoromethanesulfonimidate (LiTFSI)-1,3-dioxolane (DOL)/1,2-dimethoxyethane (DME) electrolyte with Li polysulfide and $LiNO_3$, which rendered more stable cycling [42].

3 Nanoscale interfacial engineering

Besides artificial SEI formation, nanoscale interfacial engineering is another important concept for the surface protection of anodes. In contrast to artificial SEIs engineered directly on the Li metal surface, nanoscale interfacial engineering aims to design and fabricate nanoscale interfaces on the current collectors. Because Li can be pre-stored in many cathode materials, it is valid to design an anode starting without Li, which offers several advantages. First, nanoscale interfacial layers can be fabricated regardless of the high reactivity of Li metal, which often limits the fabrication of artificial SEIs on Li metal surfaces. The strategy greatly extends the range of nanofabrication techniques suitable for engineering nanoscale interfacial layers, offering many more possibilities. Second, since no Li is present at the anode side, minimal corrosion occurs prior to cycling, thereby guaranteeing the long-term electrochemical stability of the cell in storage. Third, once Li is deposited onto the anodes, the SEI can spontaneously form with support from the nanoscale interfacial layer, reinforcing the SEI without severe fracture.

Cui et al. first demonstrated this concept by fabricating a thin film of interconnected carbon nanospheres on a Cu current collector as the anode [43]. Unlike the bare Cu surface, which forms an unstable SEI prone to cracking and dendritic growth (Fig. 2(a), top), the carbon nanosphere thin film serves as a flexible and robust support for the SEI, preventing fractures by high interfacial fluctuation (Fig. 2(a), bottom). The comparison of Li morphologies with and without the carbon nanosphere thin film is shown in Figs. 2(b) and 2(c), respectively, where dendritic Li is observed on the bare Cu foil and columnar Li is obtained on the carbon nanosphere-modified Cu foil. The Li deposition behavior below the carbon nanospheres is later visualized by *in situ* transmission electron microscopy (TEM) (Figs. 2(d) and 2(e)), which shows that carbon nanospheres are lifted up by the deposited Li.

Two-dimensional (2D) materials such as hexagonal boron nitride (h-BN) and graphene have recently attracted extensive attention [44]. Because they have good mechanical properties and outstanding electrochemical stabilities, they exhibit great potential as interfacial layers for stabilizing Li metal. It has been reported that a thin h-BN layer (Figs. 2(f) and 2(g)) grown directly on Cu foil can stabilize an as-formed SEI and promote much more uniform Li deposition underneath. SEM images obtained after 10 galvanostatic cycles indicate a less porous and more uniform Li deposition for the case with h-BN layers than that for the unmodified current collector (Figs. 2(h) and 2(i)). In addition to h-BN, surface graphene layers obtained by direct chemical vapor deposition (CVD) on Cu also demonstrated efficacy in the same report.

Polymeric interfacial layers are also of great interest because they can possess elastic or flowable natures. For polymer coatings on Li metal, however, the choice of polymer is highly limited because many

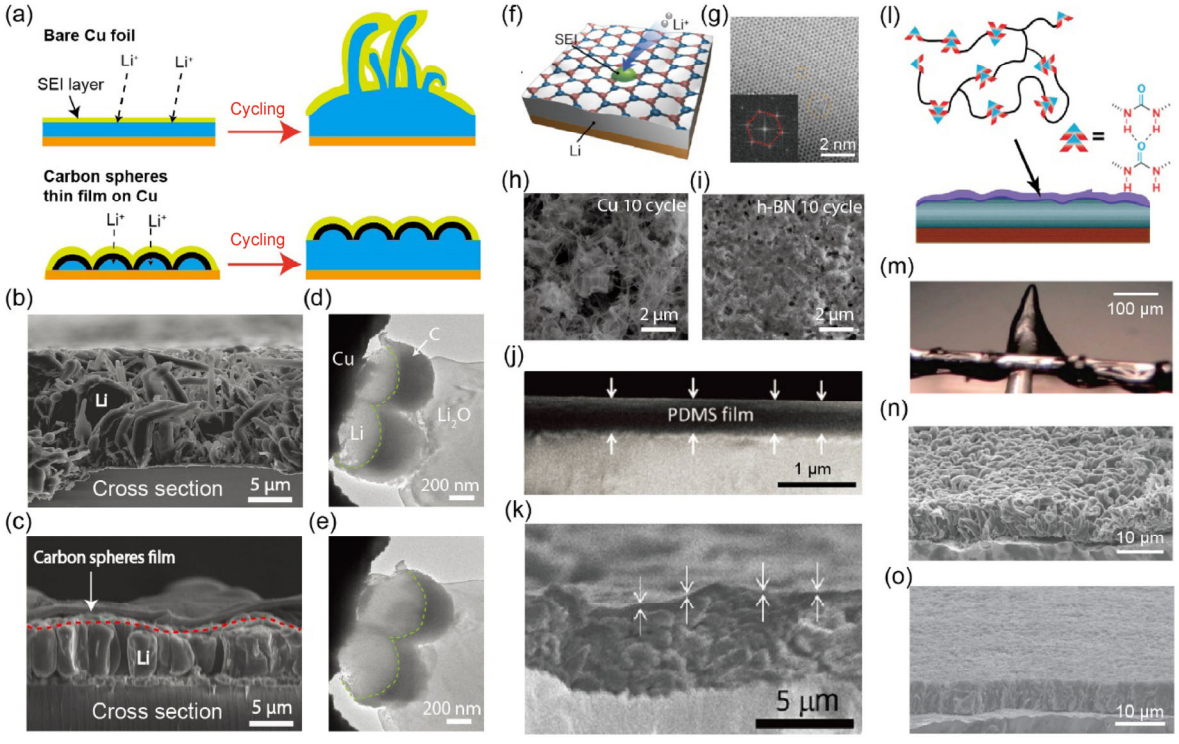

Figure 2 (a) Schematic showing the Li deposition behavior on Cu foil (top) and Cu foil modified with a thin film of interconnected carbon spheres (bottom), where the modified Cu foil exhibits more uniform Li deposition (reproduced with the permission from [43], © Nature Publishing Group 2014). (b) A cross-sectional SEM image showing the Li deposited on the Cu foil exhibiting dendritic form (reproduced with the permission from [43], © Nature Publishing Group 2014). (c) A cross-sectional SEM image showing the Li deposited beneath the film of carbon spheres, having columnar rather than dendritic morphology (reproduced with the permission from [43], © Nature Publishing Group 2014). (d) and (e) *In-situ* TEM images of Li deposited onto carbon sphere-modified Cu at 1 (d) and 32 s (e), where the carbon spheres are lifted by the underlying deposited Li (reproduced with the permission from [43], © Nature Publishing Group 2014). (f) Schematic of h-BN grown directly on Cu foil as a nanoscale interface (reproduced with the permission from [44], © American Chemical Society 2014). (g) HR-TEM image of monolayer h-BN film with hexagonal lattice (reproduced with the permission from [44], © American Chemical Society 2014). Inset: fast Fourier transform (FFT) of TEM image, showing a single set of hexagonal spot patterns. (h) and (i) SEM images showing the surface Li morphology on bare Cu (h) and h-BN-coated Cu (i) after 10 cycles at 0.5 $mA \cdot cm^{-2}$ (reproduced with the permission from [44], © American Chemical Society 2014). (j) A cross-sectional SEM image showing a PDMS coating on Cu foil as a nanoscale flexible interfacial layer (reproduced with the permission from [45], © WILEY-VCH Verlag GmbH & Co. KGaA, Weinheim 2017). (k) A cross-sectional SEM image showing the Li deposited underneath the PDMS film on Cu foil at 0.5 $mA \cdot cm^{-2}$ (reproduced with the permission from [45], © WILEY-VCH Verlag GmbH & Co. KGaA, Weinheim 2017). (l) Schematic of soft and flowable polymer coated on Cu foil (reproduced with the permission from [46], © American Chemical Society 2016). (m) Digital photo showing that the viscoelastic polymer can withstand needle puncture without breaking (reproduced with the permission from [46], © American Chemical Society 2016). (n) and (o) SEM images comparing the deposited Li morphologies on bare Cu foil (n) and viscoelastic polymer-coated Cu foil (o) (reproduced with the permission from [46], © American Chemical Society 2016).

solvents used in the processing of polymers can react vigorously with Li. Engineering the layer directly on current collectors circumvents this issue and offers more possible material choices. In this scenario, a poly(dimethylsiloxane) (PDMS) interfacial layer with nanopores (Fig. 2(j)) was demonstrated by Zhu et al. [45]. After Li plating, Li was confined under the PDMS layer and well protected (Fig. 2(k)). Additionally, a soft and flowable polymer with hydrogen bonding sites was developed by Cui and Bao et al. for stabilizing the SEI (Fig. 2(l)) [46]. The viscoelastic polymer effectively prevents puncturing by sharp needles, as shown in Fig. 2(m). Even when broken, the polymer promptly self-heals, affording a pinhole-free film. These properties offer unique opportunities to stabilize the SEI, homogenize Li deposition, and withstand Li dendrite penetration. As a consequence, a much denser and more homogenous deposited Li is obtained

(Figs. 2(n) and 2(o)). In addition, a composite of inorganic particles and polymers can also be a promising interfacial layer [47] possessing good flexibility and a higher modulus.

4 Three-dimensional current collector for Li metal

As a key battery component, the current collector also plays a profound role in Li metal anode behavior. It affects the nucleation at the initial stage of Li plating as well as the distribution of current density and electric field, both of which influence the morphology of Li deposition. Conventional anode current collectors used in Li batteries, such as Cu and Li foils, have planar configurations, which generate inhomogeneity in the Li-ion flux under relatively high current densities. To overcome this limitation, several studies have employed three-dimensional (3D) porous metal current collectors to accommodate Li deposition. Current collectors with significantly increased electroactive surface areas can significantly reduce the local effective current density; therefore, the approach generally promotes more uniform Li deposition with suppressed dendrite formation. Dendrites that do grow are better confined inside 3D current collectors, with alleviated risks of piercing the separator. Guo et al. fabricated a submicrometer-sized Cu skeleton via the reduction of $Cu(OH)_2$ fibers grown on Cu foil [48]. For a planar Cu foil, the Li deposits during the nucleation step resemble charge centers that locally enhance the Li-ion flux, thereby amplifying dendrite growth; meanwhile, the numerous protuberant tips on the 3D Cu current collector all serve as nucleation sites, affording a more homogeneously distributed electric field (Fig. 3(a)). In an ether electrolyte, Li was observed to deposit within the pores of the 3D Cu current collector, providing a relatively flat Li surface (Fig. 3(b)) and improved cycling performance. Similarly, Yu and Yao et al. developed a free-standing Cu nanowire (NW) network by solvent evaporation-assisted assembly to envelop Li deposition (Figs. 3(c) and 3(d)) [49]. With the suppressed Li dendrite growth and the high conductivity of Cu NW network, the high CE of 98.6%, averaged over 200 cycles, was achieved in an ether electrolyte at a current density of 1 $mA·cm^{-2}$, showing reduced and stable voltage hysteresis. Other representative works on current collectors include the development of porous Cu by dealloying bimetallic Cu–Zn [50], Li_2O-reinforced Cu nanoclusters [51], Ni foam-based Li anodes [52], and stainless-steel fibrous metal felt interlayers on Li foil [53].

Compared to metallic current collectors, carbon-based current collectors have the advantages of light weight, high electrical conductivity, good mechanical strength, and large specific surface area. Stucky et al. developed spatially heterogeneous carbon fiber papers as surface dendrite-free current collectors for Li deposition [54]. Notably, an insulating layer composed of SiO_2 and SiC was specially introduced on the electrolyte-facing surface of the carbon fiber paper by line-of-sight deposition, ensuring that Li plating was well-confined inside the porous 3D current collector without forming dendrites directly on the top surface (Fig. 3(e)). A CE of ~94% was achieved at the current density of 2 $mA·cm^{-2}$ and a deep Li deposition of 4 $mA·h·cm^{-2}$ in a carbonate electrolyte. Zhang et al. proposed graphene-based 3D current collectors with different nanostructural designs, including reduced graphene oxide (rGO) foams [55] and unstacked 3D hexagonal graphene flakes [56]. The Li plating behavior on the unstacked graphene flakes is illustrated in Fig. 3(f). Because of the ultralow local current density, Li ions tend to migrate through the SEI and deposit homogeneously on the graphene flakes, which not only inhibit dendrite formation (Fig. 3(g)) but also improve the CE by preventing repeated SEI breakdown and repair. As a result, in a LiTFSI–lithium bis(fluorosulfonyl)imide (LiFSI) dual-salt ether electrolyte, Li cycling at a current density of 0.5 $mA·cm^{-2}$ (0.5 $mA·h·cm^{-2}$) using a current collector of unstacked graphene flakes could realize a CE of ~93% for at least 50 cycles, while that of a Cu foil anode fluctuated between 65% and 85%. In addition, nanostructures such as 3D graphene-coated Ni foam, 3D carbon nanotube (CNT) film [57], and massive artificial graphite have also been proposed [58, 59], in which improved CE and well-controlled Li deposition were demonstrated.

Besides engineering nanostructures as advanced current collectors, replacing Li foil with higher-surface-area Li is another alternative to dissipate

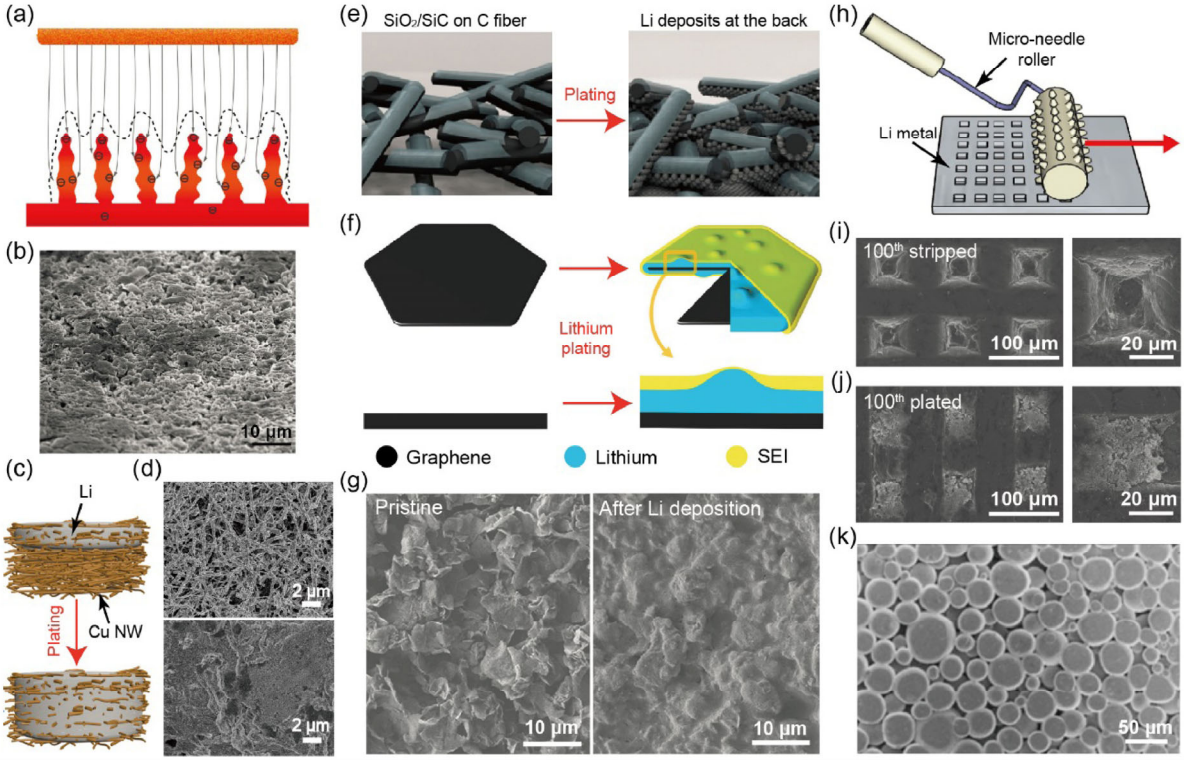

Figure 3 (a) Illustration of the proposed electrochemical deposition processes of Li metal on a 3D current collector, in which the distribution of electrons and the possible Li deposition positions (dashed lines) are shown (reproduced with the permission from [48], © Nature Publishing Group 2015). (b) Side-view SEM image of Li deposited under 2 mA·h·cm^{-2} on the 3D Cu current collector (reproduced with the permission from [48], © Nature Publishing Group 2015). (c) Illustration of Li deposition into Cu NW network current collector (reproduced with the permission from [49], © American Chemical Society 2016). (d) SEM images of the Cu NW current collector with 2.5 mA·h·cm^{-2} (top) and 7.5 mA·h·cm^{-2} (bottom) Li plating (reproduced with the permission from [49], © American Chemical Society 2016). (e) Schematic of Li deposition confined within the voids of spatially heterogeneous carbon fiber paper (reproduced with the permission from [54], © Elsevier B.V. 2012). (f) Schematic of Li plating process on one graphene fl(f) (reproduced with the permission from [56], © WILEY-VCH Verlag GmbH & Co. KGaA, Weinheim 2016). (g) SEM images of the pristine graphene flake current collector (left) and the current collector after 2 mA·h·cm^{-2} Li deposition (right) (reproduced with the permission from [56], © WILEY-VCH Verlag GmbH & Co. KGaA, Weinheim 2016). (h) Schematic of the micro-needle technique for Li foil surface patterning (reproduced with the permission from [60], © WILEY-VCH Verlag GmbH & Co. KGaA, Weinheim 2015). SEM images of the stamp-patterned Li metal after 100 galvanostatic (i) stripping cycles and (j) plating cycles at a current density of 2.4 mA·cm^{-2} (0.2 mA·h·cm^{-2}) (reproduced with the permission from [61], © WILEY-VCH Verlag GmbH & Co. KGaA, Weinheim 2016). (k) SEM image of Li powder (reproduced with the permission from [64], © WILEY-VCH Verlag GmbH & Co. KGaA, Weinheim 2014).

the local current density and achieve better cycling performance. Mechanical micro-patterning of Li foil surfaces has been demonstrated using both commercialized micro-needle rollers (Fig. 3(h)) and stainless-steel stamps [60, 61]. With the surface area thus increased, the patterned Li metal electrodes showed reduced polarization and improved rate performance in half cells. Moreover, the patterned cavities served as preferential Li plating sites, permitting the electrode to maintain its original structure even after 100 galvanostatic cycles (Figs. 3(i) and 3(j)). Finally, Li metal anodes based on coated Li metal powders can also provide increased active surface areas (Fig. 3(k)) [62–64]. However, careful handling of the Li powder is required, as it is highly reactive.

Finally, although the Li deposition behavior can be much better controlled by employing 3D current collectors, it remains challenging to achieve sufficiently high CE for practical applications. This can be attributed to the lack of surface protection, especially when depositing Li onto high-surface-area current collectors. Therefore, current collector engineering could be more

promising when used in conjunction with surface passivation methodologies, such as artificial SEI coatings.

5 Enabling uniform Li-ion flux by polar buffer layers

Since spatial inhomogeneity in Li-ion distributions on electrode surfaces contributes directly to Li dendrite formation, the rational design of nanofibrous buffer layers has been explored recently to achieve more uniform Li-ion flux. Generally, buffer layer materials possess high densities of polar surface functional groups to ensure sufficient electrolyte intake, thereby realizing better electrode–electrolyte contact than that attained using conventional polyethylene separators alone. In addition, strong interactions between the polar buffer layer and Li ions slow the movement of Li ions towards deposition hot spots, such as Li dendrites or protuberances of Cu current collectors, thereby promoting more uniform Li deposition. For example, Cui et al. modified Cu foil current collectors with a 3D oxidized polyacrylonitrile (PAN) nanofiber layer (Fig. 4(a)) [65]. As can be seen from the SEM image (Fig. 4(b)), after Li plating at the current density of 3 mA·cm^{-2} for 1 h, the Li is completely confined within the oxidized PAN nanofiber layer; no dendrites can be observed outside the layer. In an ether electrolyte, the CE in the presence of the oxidized PAN nanofiber layer achieves an average value of 97.4% over 120 cycles at the current density of 3 mA·cm^{-2} (1 mA·h·cm^{-2}), while that of a pristine electrode deteriorated rapidly within merely 50 cycles. In another study, Zhang et al. employed polar glass fiber cloths as buffer layers (Fig. 4(c)), which also promoted uniform Li deposition (Fig. 4(d)) and greatly enhanced the CE (98%, 97%, 96%, 93%, and 91% under the current densities of 0.5, 1.0, 2.0, 5.0, and 10.0 mA·cm^{-2}, respectively, with the areal capacity of 0.5 mA·h·cm^{-2}) in an ether electrolyte [66]. Other buffer layer materials have also been studied, including carbon nanofibers, CNTs, and polyaniline–CNT composites [67–70].

6 Nanoscale scaffolds as stable hosts for pre-storing Li

The high reactivity and the virtually infinite relative volume change during cycling are the two root causes of all the challenges associated with Li metal anodes. Though various different approaches have been proposed to stabilize the Li–electrolyte interface, the importance of maintaining constant Li anode

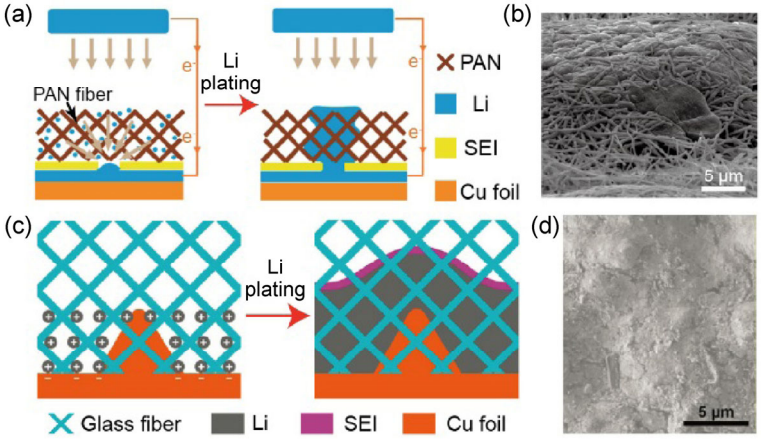

Figure 4 (a) Schematic of Li deposition on oxidized PAN nanofiber-modified Cu. The strong interaction between Li ions and the nanofibers hinders Li ions from concentrating around the "hot spots", enabling a relatively homogeneous Li deposition (reproduced with the permission from [65], © American Chemical Society 2015). (b) SEM image showing that Li deposition can be confined inside the oxidized PAN nanofiber layer without dendrite formation (reproduced with the permission from [65], © American Chemical Society 2015). (c) Schematic showing that the Li ions concentrated by the protuberances on the Cu foil electrode can be redistributed by the polar glass fiber cloth, rendering dendrite-free Li deposition (reproduced with the permission from [66], © WILEY-VCH Verlag GmbH & Co. KGaA, Weinheim 2016). (d) SEM image of Li deposits (2.0 mA·h cm^{-2}) on the glass fiber-modified Cu foil (reproduced with the permission from [66], © WILEY-VCH Verlag GmbH & Co. KGaA, Weinheim 2016).

dimensions has long been overlooked. Large volume variation induces mechanical instability in fragile SEI layers, causing continuous side reactions and uneven Li deposition. Moreover, floating electrode–separator interfaces can damage cells, creating potential safety hazards and tremendous engineering challenges for implementing batteries in confined spaces.

Spearheaded by Cui et al., stable hosts have recently been introduced to Li metal via molten Li infusion in an effort to minimize anodic volume change during electrochemical cycling [18, 71, 72]. The host materials must satisfy several important criteria: (1) sufficient mechanical properties to sustain a constant electrode volume during cycling; (2) good chemical and electrochemical stability against Li; (3) light weight and high surface area for efficient Li intake. Carbon is among the lightest materials available for scaffold construction. Therefore, in one study, various carbon materials were screened; rGO was found to possess a unique molten Li wettability, or lithiophilicity [18]. When contacting molten Li, densely stacked GO film can be rapidly reduced via a "spark reaction", simultaneously creating nanogaps between the rGO layers. Fast and uniform Li infusion can be accomplished in the subsequent step by placing the edge of the rGO film in molten Li, because of the synergetic effects of the lithiophilic nature of sparked rGO and the capillary force of the nanogaps (Figs. 5(a) and 5(b)). Cross-sectional SEM images of the resulting layered Li–rGO composite electrode during Li stripping/plating are shown in Figs. 5(c)–5(e), where Li is observed to cycle in and out of the interlayer gaps. With the rGO host, the dense Li can be divided into finer domains, which effectively reduces the thickness fluctuation to only ~20%. In addition, a high-surface-area Li anode can be obtained, which significantly reduces the effective current density during cycling. Therefore, much more stable cycling with low hysteresis occurs

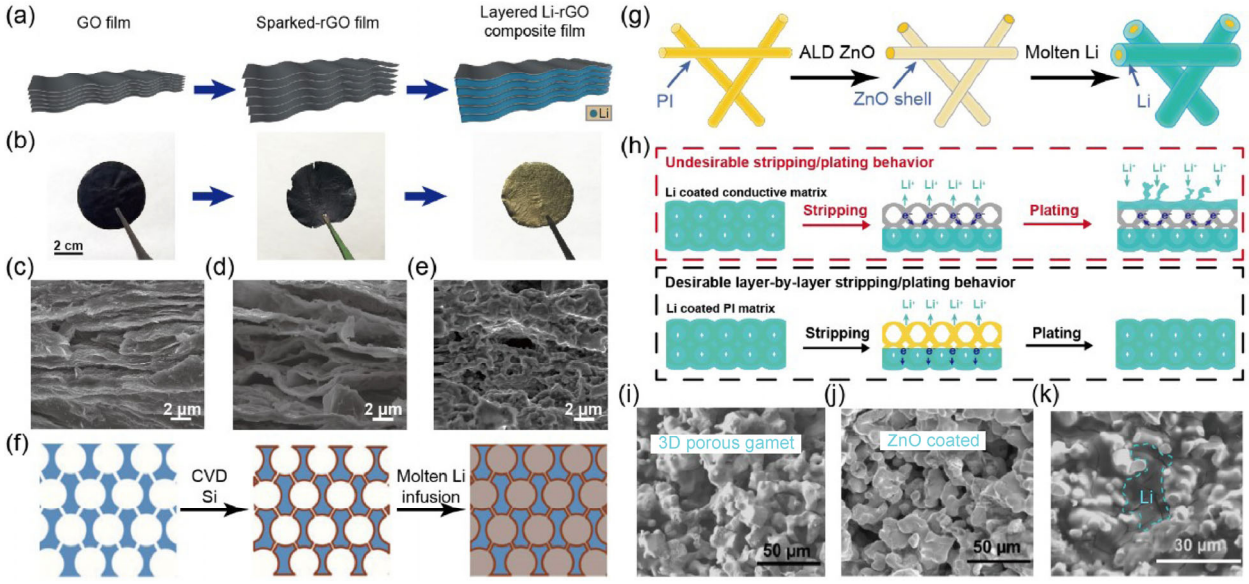

Figure 5 (a) Schematic of the fabrication process for the layered Li–rGO composite electrode and (b) corresponding digital camera images (reproduced with the permission from [18], © Nature Publishing Group 2016). (c)–(e) Cross-sectional SEM images of the layered Li–rGO electrode (c) before and (d) after Li stripping, and (e) after one stripping/plating cycle (reproduced with the permission from [18], © Nature Publishing Group 2016). (f) Schematic of Si-coated scaffold for molten Li infusion (reproduced with the permission from [71], © National Academy of Sciences 2016). (g) Schematic of the fabrication process of the Li-coated PI matrix via ALD ZnO surface modification (reproduced with the permission from [72], © Nature Publishing Group 2016). (h) Schematic demonstrating the undesirable Li stripping/plating behavior with a highly conductive host material, where Li tends to deposit directly on the top surface, leading to volume change and dendrites shooting out of the matrix, and the desirable layer-by-layer stripping/plating behavior with a non-conductive host material (reproduced with the permission from [72], © Nature Publishing Group 2016). Cross-sectional SEM images of (i) pristine and (j) ZnO-coated porous garnet with a porosity of 60%−70%. (k) Cross-sectional SEM image of Li-infiltrated porous garnet after ZnO surface treatment, where almost all pores have been filled by Li (reproduced with the permission from [75], © American Chemical Society 2017).

in both symmetric-cell and full-cell configurations, even in a carbonate-based electrolyte.

Excellent lithiophilicity of the host materials is necessary for molten Li infusion, yet few materials exhibit intrinsic lithiophilicity similar to that of rGO. To expand the choices for host materials, Cui et al. demonstrated a versatile surface modification strategy. In one case, porous scaffolds were rendered lithiophilic by a thin (~30-nm) Si coating by CVD (Fig. 5(f)), attributed to the chemical reaction between Si and molten Li that generates more lithiophilic species (Li_xSi) *in situ* on the scaffold surface [71]. A composite Li anode was fabricated from a Si-coated carbon nanofiber network, from which minimal electrode volume change and improved electrochemical performance were achieved. In another representative work, a ZnO coating via ALD also demonstrated effective lithiophilicity [72]. After coating ZnO (~30 nm) onto electrospun heat-resistant polyimide (PI) nanofibers, molten Li is easily infused into the matrix, forming a nanoporous Li electrode by the formation of Li_xZn/Li_2O (Fig. 5(g)). In addition, it is noted that constructing the host with a non-conductive polymeric framework can be beneficial for confining the Li metal during later cycles (Fig. 5(h)). For instance, if the host is highly conductive, such that electrons are easily transported to the electrolyte-facing top surface during plating, the deposition of Li outside the host and thus inefficient Li confinement may occur because of the high availability of both electrons and Li ions, especially at high current densities. In contrast, for a host built with non-conductive materials, Li is the only conductive species within the host. As a consequence, electrons are transported exclusively by the unstripped Li at the bottom, preventing the direct deposition of Li on the very top of the anode. Other materials that can chemically react with Li may also serve as lithiophilic coatings.

Compositing Li with Li-containing alloys has also been investigated as an alternative to obtain nanostructured Li anodes. For example, a Li-rich multiphase alloy foil with the nominal composition $Li_{2.6}BMg_{0.05}$ demonstrated a reduced tendency for dendrite formation, lower polarization, and more stable electrochemical performance, compared to pure Li foil [73]. Similar effects have also been observed with metallic Li contained in a fibrous Li_7B_6 matrix [74]. Given the vast choice of possible materials (oxides, sulfides, nitrides, etc.), it is worthwhile at the current stage to screen them broadly in order to find ideal hosts for Li metal.

Notably, confining Li in 3D hosts increases the surface area of the Li metal, which can promote more side reactions, especially during the initial cycles. Thus, engineering a stable 3D Li–electrolyte interface is necessary to boost the performance of 3D Li for practical applications [39]. Ultimately, combining nanostructured Li with the proper solid electrolyte may be the best way to achieve a stable Li–electrolyte interface. In addition to the necessity of improving the ionic conductivity and electrochemical stability of current solid electrolytes, concentrated efforts must also address the fundamental issue of wettability between solid electrolytes and Li metal. Recently, Hu et al. demonstrated the successful infiltration of Li into a porous garnet-type solid electrolyte host by modifying the surface with ALD ZnO (Figs. 5(i)–5(k)) [75]. The reaction between the molten Li and the ZnO coating afforded improved Li–solid electrolyte contact, which caused a decrease by one order of magnitude in the interfacial resistance compared to that in the uncoated electrolyte. Si and Al_2O_3 coatings on garnet-type solid electrolytes have also demonstrated efficacy in improving the Li–solid electrolyte contact [76, 77].

It should be acknowledged that the transformation from 2D Li foil to 3D forms of Li entails some sacrifice of the battery's energy density, but we believe this is necessary to solve the intrinsic problems of Li foil, such as the infinite relative volume change and sluggish kinetics. A trade-off between energy density and safety and power density must be made. As a consequence, it is also important to further modify the structure of 3D Li to solve these problems with minimal sacrifice of energy density.

7 Guided Li deposition by heterogenous seeds

For Li full cells with Li-containing cathodes, the anode can ideally begin as an empty scaffold in which Li is deposited during battery charging. Nonetheless, it is

challenging to realize spatial control over Li deposition because of the randomness of Li nucleation and growth. Recently, Cui et al. explored Li deposition on various metal substrates and discovered a substrate-dependent Li nucleation behavior [78]. In the study, an appreciable nucleation overpotential was observed for Li deposition on metals with negligible solubility in Li, such as Cu (Fig. 6(a)). However, no nucleation barriers were seen when Li was deposited on substrates with definite solubilities in Li, such as Au (Fig. 6(b)). The difference in nucleation overpotential therefore enables the spatially controlled deposition of Li metal. Accordingly, they rationally designed a nanocapsule structure for a Li metal anode, consisting of hollow carbon spheres with Au nanoparticle seeds inside, such that Li metal can predominantly grow within the nanocapsules during deposition (Fig. 6(c)). The selective deposition process was confirmed by *in situ* TEM (Figs. 6(d) and 6(e)). The encapsulation by the hollow carbon spheres stabilized the SEI and eliminated dendrite formation; as a result, 98% CE over more than 300 cycles was realized in a corrosive carbonate electrolyte. In addition to metal nanoparticle-seeded growth, N-doped few-layer graphene islands on insulating polymer-coated Cu have also been employed to realize the spatial control of Li deposition [79].

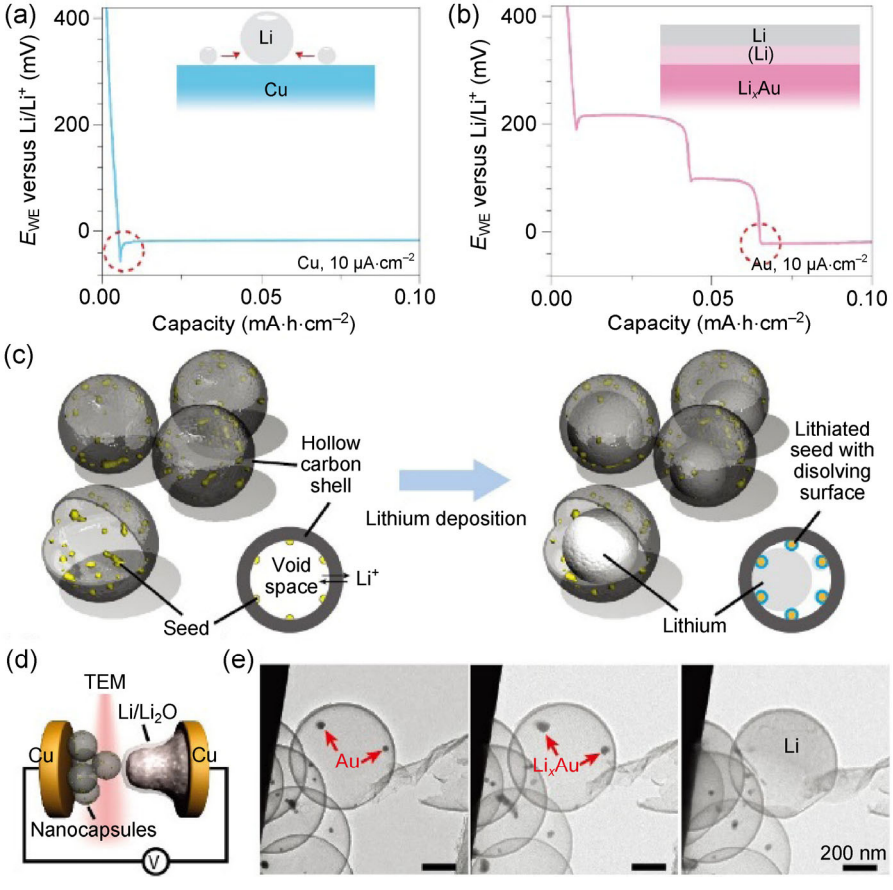

Figure 6 (a) Voltage profiles of galvanostatic Li deposition on Cu at a current density of 10 μA·cm^{-2}. A clear overpotential is observed, as circled by the dashed line. Inset: schematic of the mechanism of Li nucleation, which explains the extra energy involved. (b) Voltage profiles of galvanostatic Li deposition on Au at a current density of 10 μA·cm^{-2}; as indicated by the dashed circle, no overpotential is observed at the onset of Li metal plating. Inset: schematic showing how the dissolution of the solid-solution buffer layer of Au in Li reduces the nucleation energy. (c) Schematic showing the design of nanocapsules with Au nanoparticles embedded in the inner walls of carbon spheres for confining Li metal. (d) Schematic of dry cell for *in-situ* TEM Li deposition study. (e) TEM snapshots of the Li deposition process inside Au-seeded hollow carbon spheres during *in-situ* Li metal plating. Reproduced with the permission from [78], © Nature Publishing Group 2016.

8 Confinement of Li metal by vertically aligned channels

Vertically aligned channels have the potential to confine Li metal without permitting dendritic propagation. It is known that, for a planar Li foil, the formation of a Li nucleus concentrates additional Li ions on the foil, promoting uneven Li deposition and the further growth of the nuclei. This is a result of the high availability of Li ions from all directions around the nucleus; ions are attracted by both tip-enhanced electric fields and geometrical effects [80, 81]. Simulation results have illustrated that, by patterning vertically aligned channels on the current collector, the Li-ion flux could be equalized in each channel [82]. A nucleus that grows more quickly initially in one channel would not attract a concentrated Li-ion flux. Instead, the Li-ion flux in each channel would remain roughly constant. This design offers the opportunity to average the deposited Li across all channels, rather than inducing locally favorable plating.

It was previously found that anodized TiO_2 nanochannel arrays can be used as Li metal storage media [83]. Figure 7(a) shows the structure and Li deposition behavior of TiO_2 nanochannel arrays. Li is successfully confined within the channels (Fig. 7(c)) rather than depositing in dendritic form (Fig. 7(b)). In addition to vertically aligned TiO_2 channels, anodic aluminum oxide has also been frequently used to offer either Li-ion flux orientation or Li metal confinement [84–86]. However, oxide nanochannel arrays have the drawback of side reactions between the oxides and Li. Li can be gradually consumed within the cell, which makes the materials less practical. Later, PI-based nanochannel arrays were developed (Fig. 7(d)) [82]. The top-view and cross-sectional SEM images of the PI nanochannels are shown in Figs. 7(e) and 7(f), respectively. The PI-based arrays possess several distinguishing advantages, including excellent chemical stability vs. Li, high mechanical strength, and good electrolyte wettability. These advantages guarantee minimal side reactions with Li, high mechanical stability during Li deposition, and good electrolyte accessibility in all channels. As shown in Fig. 7(g), the deposited Li is distributed evenly in the channels.

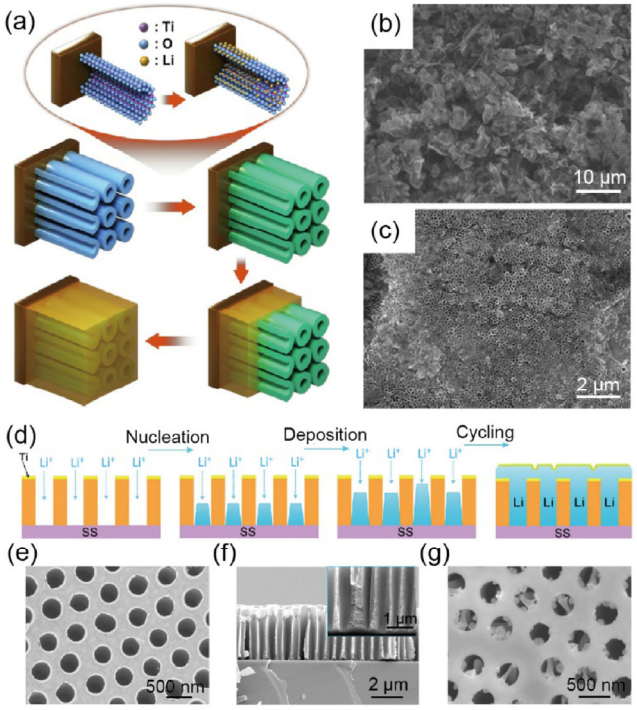

Figure 7 (a) Schematic showing the vertically oriented TiO_2-nanotube arrays as Li metal storage medium (reproduced with the permission from [83], © Elsevier B.V. 2014). (b) Surface morphology of deposited Li on a Cu substrate after 50 cycles (reproduced with the permission from [83], © Elsevier B.V. 2014). (c) TiO_2-nanotube array with deposited Li after 50 cycles (reproduced with the permission from [83], © Elsevier B.V. 2014). (d) Schematic of PI nanochannels on stainless steel for Li metal confinement (reproduced with the permission from [82], © American Chemical Society 2016). (e) and (f) SEM images showing the top (e) and cross-sectional (f) views of nanochannels (reproduced with the permission from [82], © American Chemical Society 2016). (g) Top-view SEM images showing the nanochannels with deposited Li inside the channels (reproduced with the permission from [82], © American Chemical Society 2016).

9 Separator engineering for dendrite suppression

The separator is a critical battery component that contributes to both the safety and kinetics. Its properties have direct influence on the overall battery cyclability, roundtrip efficiency, and thermal dissipation. For Li metal batteries, the separator plays an even more important role in distributing the Li-ion flux and blocking Li dendrite evolution. In the conventional Li-ion battery industry, polyolefin-based (e.g., polypropylene (PP) and polyethylene (PE)) separators

dominate the market because they offer economical manufacturing and good overall performance in Li-ion system [87]. However, pure polyolefin separators cannot easily satisfy the more restrictive standards imposed by Li metal batteries. On one hand, Li metal systems require separators with excellent electrolyte wettability; otherwise, the uneven accessibility of Li-ions to the Li metal surface would exacerbate locally favorable Li nucleation and deposition, which eventually cause dendritic formation. On the other hand, a separator with a much higher modulus is preferred as a physical barrier to block Li dendrite penetration. Even though much effort has been devoted in electrode design to suppress Li dendrite formation, full inhibition cannot yet be achieved at this stage, especially in more intensive operation conditions, such as high power and low temperatures. In this context, multiple strategies have been developed to improve separators for Li metal cells.

9.1 Improving electrolyte wettability and regulating surface tension

Conventional polyolefin usually exhibits moderate electrolyte wettability, which can be attributed to the non-polar nature of the polymer chains. Insufficient wettability of the separator can cause uneven Li-ion distribution at the interface of the Li metal electrode, exacerbating uneven Li deposition. Choi et al. developed a polydopamine coating on a conventional PE separator to afford improved electrolyte wettability (Fig. 8(a)) [88]. More uniform Li deposition behavior was observed with the coated separator compared to that with an unmodified PE separator (Fig. 8(b)). In addition to the polydopamine modification approach, inorganic materials [89–92], PI [93, 94], and cellulose-based separators [95, 96] were developed and shown improved electrolyte wettability. Recently, Archer et al. reported on simulation results that clarified the relationships among multiple parameters where surface tension is important [97, 98]. It was found that adequate surface chemistry for the separator can help to regulate the surface tension and suppress Li dendrite formation, even for a separator with a mediocre modulus [99]. For example, Kim et al. developed a N and S co-doped graphene coating deposited on a PE separator, which promoted more uniform and denser morphology on a cycled Li metal electrode (Fig. 8(c)) [100].

9.2 Developing ultrastrong separators

In addition to improving electrolyte wettability and regulating surface tension, the development of ultrastrong separators capable of physically suppressing Li dendrites is also of great interest. Recently, much effort has been devoted to this topic. The conventional polyolefin separator generally exhibits moderate mechanical properties. For example, a typical PP separator fabricated by the dry process of uniaxial stretching has a Young's modulus of ~150 MPa in the machine direction and ~15 MPa in the transverse direction [87]. The anisotropic modulus in two directions not only causes anisotropic shrinkage at elevated temperature, but also increases vulnerability to puncturing by either Li dendrites or metallic impurities. Utilizing high-modulus polymer materials (e.g., PI and aramids) as alternatives to polyolefin has been considered a promising strategy to afford much stronger separators. However, almost all of these high-modulus polymers exhibit poor processability. They are generally resistant to high temperatures and few solvents can be used to dissolve them. Recently, Kotov et al. developed a method to disperse Kevlar® aramid in the form of nanofibers, which enables layer-by-layer assembly to form a polyethylene oxide (PEO)/aramid nanofiber (ANF) composite membrane (Fig. 8(d)) [101]. The ultrahigh strength of the Kevlar® aramid allowed the membrane to retard even Cu dendrites (Figs. 8(e) and 8(f)), which are much stiffer than their Li counterparts. In addition to the PEO/aramid nanofibers composite membranes, pure poly(p-phenylene benzobisoxazole) (PBO) (Fig. 8(g)), also known as Zylon®, was fabricated into nanoporous membranes as a separator by Sun et al. [102]. Zylon® is an ultrastrong polymer, even stiffer than Kevlar®. A mixed acid was developed to disperse Zylon® into nanofibers, as shown in Fig. 8(h). The fabricated nanoporous membranes based on these Zylon® nanofibers exhibited high Young's moduli of ~20 ± 3 GPa (Fig. 8(i)), exceeding the threshold value predicted by Newman et al. for Li dendrite suppression [103, 104]. The membrane can be fabricated in relatively large sizes and affords good flexibility (Fig. 8(j)), which also increase the viability of application.

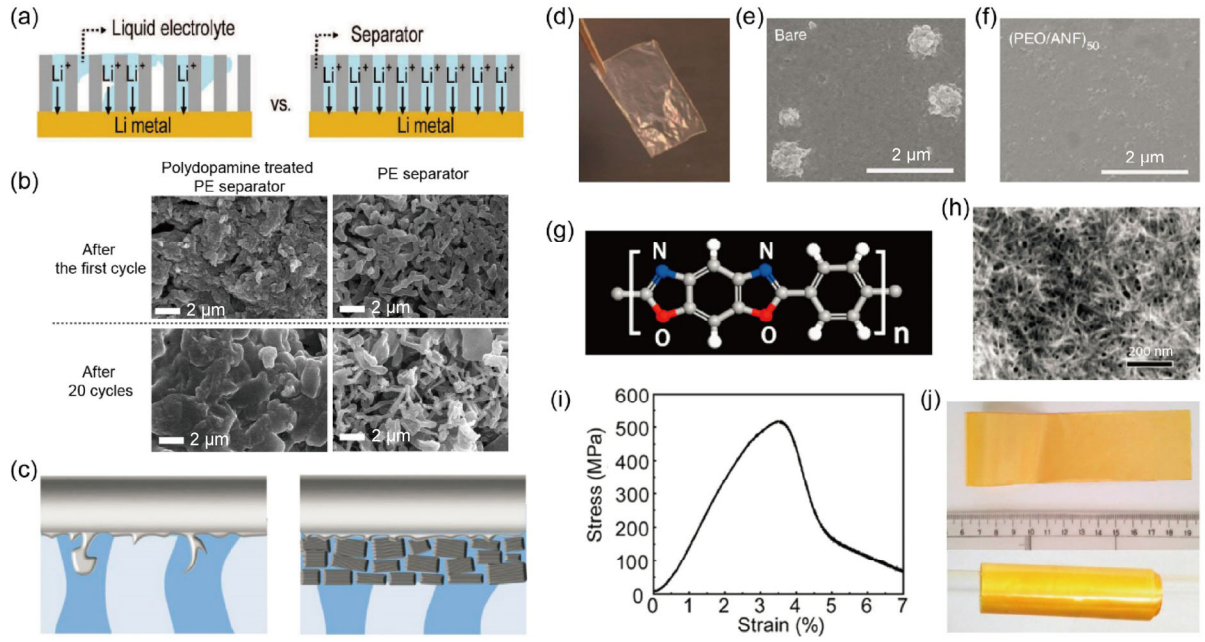

Figure 8 (a) Schematic of a normal separator with poor electrolyte wettability (left) and a polydopamine-treated separator with good electrolyte wettability (right) (reproduced with the permission from [88], © WILEY-VCH Verlag GmbH & Co. KGaA, Weinheim 2012). (b) SEM images showing the morphologies of deposited Li with (left) and without (right) polydopamine treatment after one (top) and 20 (bottom) cycles (reproduced with the permission from [88], © WILEY-VCH Verlag GmbH & Co. KGaA, Weinheim 2012). (c) Schematic of Li deposition on Li metal electrode with the PE separator (left) and N/S co-doped graphene-coated PE separator (right) (reproduced with the permission from [100], © American Chemical Society 2015). (d) Digital photo showing the PEO/ANF composite membrane (reproduced with the permission from [101], © Nature Publishing Group 2015). (e) and (f) SEM images of the bare Cu electrode (e) and Cu electrode coated with $(PEO/ANF)_{50}$ after copper dendrite growth at the current density of 10.3 $mA \cdot cm^{-2}$ (reproduced with the permission from [101], © Nature Publishing Group 2015). (g) Molecular structure of the ultrastrong PBO [102]. (h) SEM image showing the PBO nanofiber network (reproduced with the permission from [102], © American Chemical Society 2016). (i) Stress-strain curve of PBO nanoporous membrane, showing high Young's moduli of 20 ± 3 GPa (reproduced with the permission from [102], © American Chemical Society 2016). (j) Digital photos showing the large size and good flexibility of PBO nanoporous membrane (reproduced with the permission from [102], © American Chemical Society 2016).

It should be noted that it is beneficial to combine the two aspects of separator engineering together to achieve a high-performance and safe battery. By improving the electrolyte wettability and regulating the surface tension on an ultrastrong separator, improved Li diffusion and more homogenized Li deposition can be achieved, which also help to alleviate local stresses created by non-uniform surfaces.

10 Battery safety monitoring and smart functions

Safety is the first priority in Li metal batteries. Even with a well-developed Li metal electrode and the fulfillment of almost dendrite-free deposition, a single dendrite can internally short the battery and cause safety hazards. With this consideration, early warning of internal short circuits before battery failure or automatic battery shutdown before catching fire would be very helpful. In this section, we introduce a few representative strategies that have been demonstrated to achieve these goals.

In order to monitor the Li dendrite penetration process during battery cycling, Cui et al. developed a separator with dendrite detection functionality [105]. As shown in Fig. 9(a), by simply adding an electrical conducting detection layer (e.g., Cu, Al, or carbon) sandwiched by two separators, dendrite evolution can be monitored by measuring the voltage between the conducting interlayer and the anode ($V_{Cu\text{-}Li}$). Once a Li dendrite propagates from the Li anode and contacts the conducting layer, $V_{Cu\text{-}Li}$ drops to 0, signaling

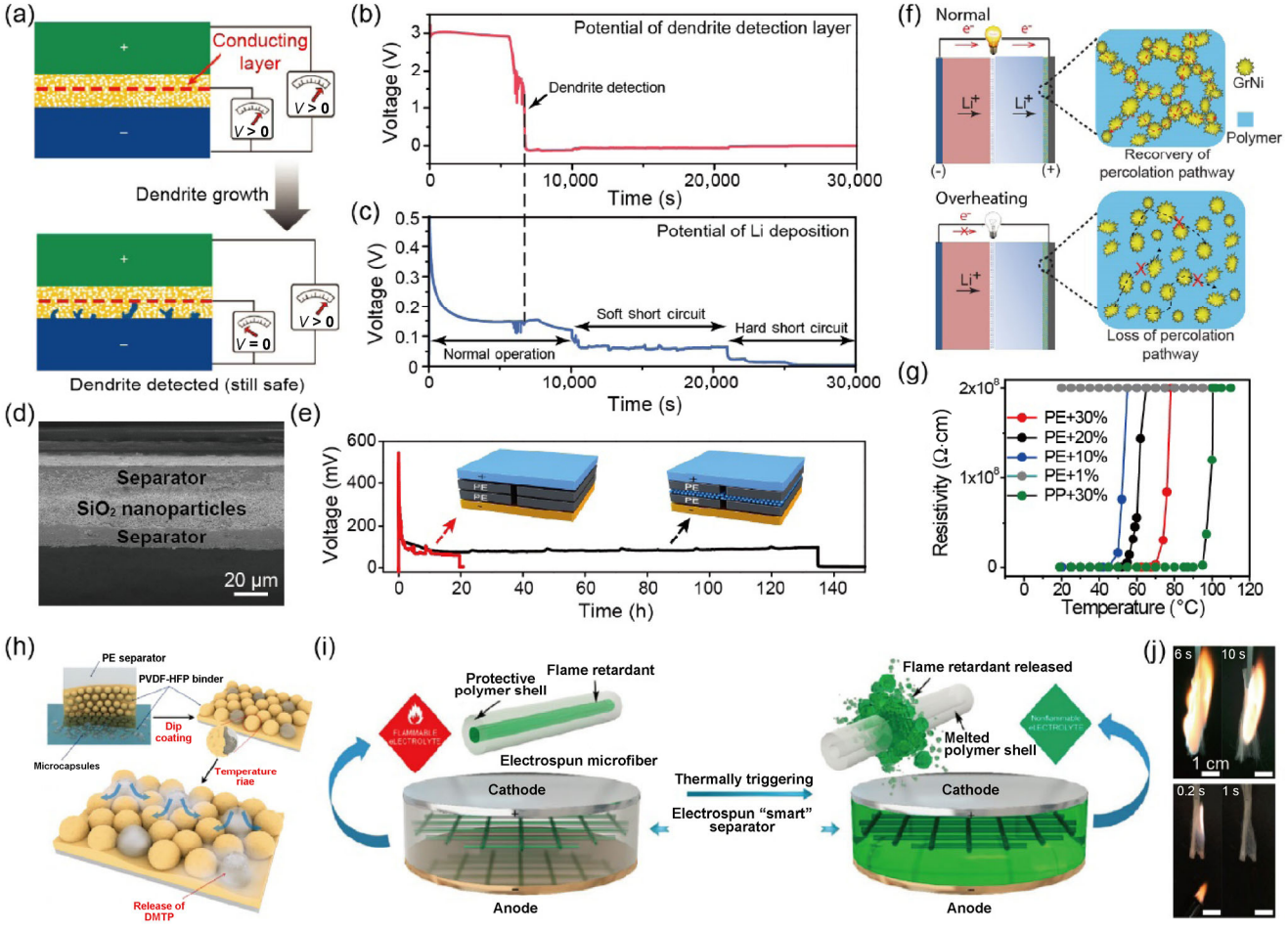

Figure 9 (a) Schematic showing the Li dendrite detection principle of a bifunctional separator. A Li battery with a bifunctional separator comprising a conducting layer sandwiched between two conventional separators, where the overgrown Li dendrite penetrates the separator to make contact with the conducting Cu layer, causing a drop in $V_{Cu\text{-}Li}$ as a warning of impending failure by an internal short circuit (reproduced with the permission from [105], © Nature Publishing Group 2014). However, the full battery remains safely operational with non-zero potential. (b) and (c) Voltage profiles showing the dendrite detection of a PI bifunctional separator. The voltage of the Cu interlayer vs. Li^+/Li ($V_{Cu\text{-}Li}$) is shown in (b), and the voltage of the whole cell ($V_{Li\text{-}Li}$) is shown in (c) (reproduced with the permission from [94], © American Chemical Society 2016). The detection layer shows an early alert of dendrite penetration prior to short-circuiting of the whole cell. (d) A cross-sectional SEM image of a SiO_2 nanoparticle-sandwiched separator, where the SiO_2 nanoparticle serves as a reactive agent to consume penetrated Li and slow or stop Li dendrite penetration (reproduced with the permission from [106], © WILEY-VCH Verlag GmbH & Co. KGaA, Weinheim 2016). (e) Voltage profiles comparing the lifetimes of symmetric cells with (black) and without (red) SiO_2 nanoparticle layers prior to short circuit, where the cell with a SiO_2 nanoparticle sandwiched separator exhibits much longer cycle life (reproduced with the permission from [106], © WILEY-VCH Verlag GmbH & Co. KGaA, Weinheim 2016). (f) Schematic showing the mechanism of thermoresponsive polymer switching (TRPS) materials in cutting off an overheated battery [107]. The polymer composite film has a high electrical conductivity at room temperature because of the quantum tunneling effect enabled by the spiky nanostructure (GrNi). On heating, the polymer matrix expands, thus separating the conductive particles, which decreases the conductivity by a factor of 10^7–10^8 and thereby cut off the electrical conducting pathway. (g) Resistivity changes of various TRPS films as a function of temperature (reproduced with the permission from [107], © Nature Publishing Group 2016). (h) Schematic showing the synthesis and operation mechanism of temperature-responsive microcapsules with embedded fire-extinguishing agents (reproduced with the permission from [108], © American Chemical Society 2015). (i) Schematic showing the separator with an encapsulated flame extinguisher that can be thermally triggered to prevent the electrolyte from catching fire (reproduced with the permission from [109], © American Association for the Advancement of Science 2017). (j) Photographs recording the burning of the electrolyte in the presence of 0 wt.% (top) and 40 wt.% TPP (bottom) (reproduced with the permission from [109], © American Association for the Advancement of Science 2017).

dendrite formation and prompting the disposal of the dangerous battery. Later, the same group developed a PI separator that incorporated a conducting layer in the middle of the single-piece separator, which enabled the fabrication of fully integrated separators with built-in dendrite detection functionality [94]. Figures 9(b) and 9(c) show the voltage profiles of $V_{\text{Cu-Li}}$ and $V_{\text{Li-Li}}$, respectively, which demonstrate the dendrite detection function. It is shown that $V_{\text{Cu-Li}}$ drops to 0 during normal battery operation in Fig. 9(c), warning of the upcoming short circuit of the battery. In addition to incorporating a conducting layer for dendrite detection, it was also reported that incorporating a layer of SiO_2 nanoparticles into the separator can efficiently stop Li dendrite propagation and significantly extend the cycle life (Figs. 9(d) and 9(e)) [106]. This is because of the high reactivity between SiO_2 and Li, whereby SiO_2 can consume Li dendrites that grow into the separator.

Developing batteries that can automatically shut down prior to thermal runaway is also very attractive. Bao and Cui et al. developed a thermoresponsive coating for a current collector to fulfill this goal [107]. The coating consisted of polyolefins possessing high thermal expansion coefficients, as well as spiky Ni nanoparticles as electrically conductive pathways. At ambient temperature, the spiky Ni nanoparticles interconnect to form a low-resistance percolation pathway. Once the battery experiences thermal runaway, the polymer matrix expands, pulling the spiky Ni nanoparticles away from each other and thereby destroying the percolation pathway and increasing the resistance by a factor of 10^7–10^8 (Fig. 9(f)). This cuts off electrical conduction between the electrode and current collector. The resistance vs. temperature plot of the film is shown in Fig. 9(g). By tuning the polymer and the amount of spiky Ni nanoparticles added, the resistance switching temperature can be tuned from 50 to 100 ℃.

Temperature change is a powerful indicator of battery failure that can not only be used to cut off the electrical pathway, but also be exploited to block Li-ion transport or release additives into the system. Recently, some works have reported on the release of flame extinguishers into the electrolyte during the thermal runaway process. Kim and Jung et al. developed a microcapsule with a poly(methyl methacrylate) shell and 1,1,1,2,2,3,4,5,5,5-decafluoro-3-methoxy-4-(trifluoromethyl)-pentane (DMTP) core; the latter is a flame extinguisher [108]. With a layer of microcapsules coating the separators, once the cell is overheated, DMTP is released to mix with the electrolyte, thereby reducing the electrolyte flammability (Fig. 9(h)). Under ambient conditions, however, DMTP is well encapsulated and does not affect the electrochemical stability of the electrolyte. Later, Cui et al. developed a poly(vinylidene fluoride-co-hexafluoropropylene) (PVDF-HFP)-based separator with embedded triphenyl phosphate (TPP) as a flame extinguisher (Fig. 9(i)) [109]. The TPP flame extinguisher can be released from the separator at elevated temperatures, rendering the electrolyte nonflammable and maintaining a safe battery. As shown in Fig. 9(j), the electrolyte without the addition of TPP burns vigorously, while that with 40% TPP is extinguished immediately after ignition.

11 Nucleation and deposition in nanoscale

One of the most striking features of electrodeposited Li metal is the extensive diversity in the nano- and microstructural morphology of electrocrystallized Li by using different electrolyte solvents, salts, and additives. The figures highlighted in this review, in addition to the body of Li metal battery electrode works published recently, illustrate a wide variety of commonly observed characteristic Li structures, including round particles, filaments and whiskers, mossy or sponge-like masses, and pillar-like or columnar grains, among others. While there is not a definitive and conclusive understanding of the reasons for the preferential formation of each Li nano- or microstructure, we can begin any discussion of Li metal deposition by first considering the extremely high reactivity of Li metal.

One explanation for different Li deposition morphologies considers the role of the as-formed SEI as a protective layer affecting the electrochemical and mechanical evolution of Li. Common electrolyte solvents are not stable with Li metal, forming heterogeneous SEI passivation layers upon contact with Li surfaces [110]. Li with brittle SEI layers formed in carbonate electrolytes tends to develop elongated

Li whiskers, whereas the more elastic and polymeric SEIs from ether-based electrolytes generate rounded, smooth Li granules.

Beyond SEI mechanics, the identities and interaction energies of the compounds that come into contact with, absorb, or are formed on Li, during deposition also affect the Li deposition morphology. Steiger demonstrated the electrodeposition of faceted crystals of Li under potentiostatic conditions (Fig. 10(a)) and concluded that the planes were thermodynamically preferred as exposed facets [111]. Various calculations of the surface energies of Li crystal surfaces relative to vacuum and the interfacial energy between Li and Li compounds have been reported [112, 113], but it is difficult to extend these results to real systems where SEI layers are homogeneous and the deposited Li grains are not highly faceted. Ultimately, it is expected that the preferred exposed surfaces, and thus the shape, of deposited Li can be adjusted by tuning the composition of the SEI or the molecules present in the electrolyte. However, no specific parameter has yet been reported that describes the complex conditions present in the Li electrodeposition system.

The final morphology of the Li metal after deposition is important for characterizing various nanoengineered electrode designs, but it is equally important to observe and study the immediate and intermediate states of Li deposition as well. Intuitively, understanding the

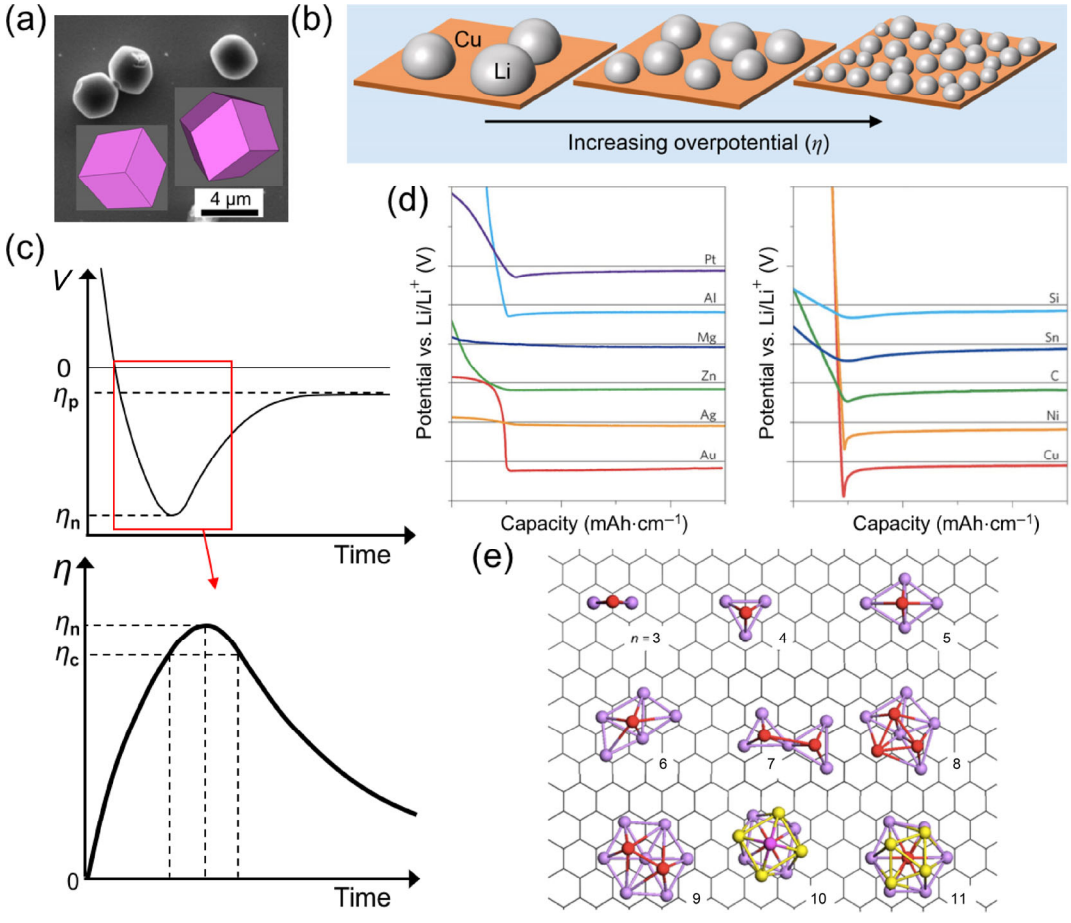

Figure 10 (a) Faceted Li particles grown at –100 mV vs. Li/Li^+ on tungsten in 1 M $LiPF_6$ in EC:DMC. (b) Schematic illustrating the decrease in Li nuclei size and increase in Li nuclei density with increasing overpotential. (c) Top: schematic of typical Li deposition voltage profile at the nucleation step. Bottom: magnified nucleation spike (flipped vertically such that negative potentials vs. Li/Li^+ are above 0) showing the critical overpotential for supercritical nuclei formation (η_c) and maximum nucleation overpotential (η_n). (d) Typical voltage profiles for Li deposition on electrode materials that exhibit some Li solubility (left) and negligible Li solubility (right) (reproduced with the permission from [78], © Nature Publishing Group 2016). (e) The most stable structures of Li atom clusters on graphene, calculated from density functional theory (reproduced with the permission from [123], © American Chemical Society 2014).

earliest stages of Li nucleation and growth may clarify the deposition process by elucidating fundamental properties and quantities, such as nucleation frequency, active site density, energy barriers, and surface energies. Various experimental and theoretical studies have explored Li nucleation in various systems.

11.1 Galvanostatic studies

Electrocrystallization of Li from an electrolyte solution proceeds by increasing the electrochemical potential of Li-ions above that of bulk metallic Li by tuning the overpotential and electrochemical supersaturation, such that forming new solid-phase Li nuclei decreases the Gibbs free energy of the system [114]. In general, battery test cells are cycled galvanostatically (constant current); as such, the majority of Li metal nucleation studies have used fixed galvanostatic currents to deposit Li. However, one critical characteristic of galvanostatic electrocrystallization is the variable electrochemical supersaturation that arises from the time-varying overpotential and prevents the derivation of an analytical expression for the nucleation rate and number of nuclei [115]. Nonetheless, galvanostatic studies represent the operating conditions of a battery and therefore can provide important and relevant information regarding Li nucleation and growth to guide the design of nanostructured electrodes. Multiple studies have observed that Li nuclei galvanostatically deposited from different electrolyte systems are decreased in size and increased in areal density as the current density is increased (Fig. 10(b)), corresponding with relationships from classical nucleation theory [116–118]. For these *ex-situ* SEM-based nucleation studies, Sano et al. used the ionic liquids of 1-propyl-1-methylpiperidinium bis(trifluoromethylsulfonyl)amide ([C_3mpip][Tf_2N]), 1-butyl-1-methylpyrrolidinium bis(trifluoromethylsulfonyl)imide ([C_4mpyr][Tf_2N]), and trimethylhexylammonium bis(trifluoromethylsulfonyl)imide ([$N_{1,1,1,6}$][Tf_2N]) [116], Iriyama et al. used LiPON solid electrolytes [117], and Cui et al. used a DOL/DME ether-based electrolyte, indicating that the expected trends occur in a variety of systems [118].

The energy barrier for Li nucleation depends on the type of working electrode. Figure 10(c) illustrates the typical voltage profile of Li deposition on a non-Li-soluble electrode at the initial stages of deposition. Initially, the voltage of the working electrode decreases to a level below the Li/Li^+ equilibrium potential by double-layer charging and adatom capacitance, until it reaches the critical overpotential, η_c, at which super-critical Li clusters form. The potential then reaches a overpotential minimum, η_n, because of the interplay between charging and nuclei growth, and finally increases to the growth overpotential plateau, η_p, as nuclei growth dominates [115]. As η_c cannot be easily extracted from voltage data, the characteristic nucleation "spike" and growth plateau overpotentials, η_n and η_p, respectively, are typically used as descriptors of Li nucleation and growth. Because of the short time scale for nucleation events to occur in galvanostatic conditions [115], the galvanostatic Li nucleation process was found to be instantaneous, with the areal nuclei density remaining constant throughout deposition [118]. Recently, Cui et al. found that substrates with some Li solubility, such as Au, exhibited little to no nucleation barrier, whereas substrates with no Li solubility, such as Cu, had much larger, exaggerated nucleation barriers (Fig. 10(d)) [78].

11.2 Potentiostatic studies

Overall, relevant studies on the initial stages of Li deposition under potentiostatic conditions are lacking. Typically, potentiostatic electrodeposition experiments are useful for measuring and calculating the fundamental properties of nucleation because the fixed polarization applies a constant driving force for electrocrystallization. Kohl et al. studied Li nuclei grown potentiostatically in organic carbonate-based ethylene carbonate (EC)/DMC and [$N_{1,1,1,4}$][Tf_2N] ionic liquid electrolytes by *ex-situ* SEM [119]. As expected, the potentiostatic conditions caused progressive nucleation, with new nuclei forming throughout the deposition process. Using a 3D model for heterogeneous hemispherical nuclei, the nuclei growth rate was calculated from the experimental data. It was found that, for Li nuclei deposited in EC/DMC, the growth rate decreased over time, whereas for the Li grown in ionic liquid, the growth rate increased, as expected. This phenomenon arose from the higher

rate of growth-impeding SEI formation in EC/DMC electrolytes as compared to that in ionic liquids. Similarly, it was found that the amount of charge needed to nucleate Li increased non-linearly with decreasing current density, implying that subcritical clusters of Li react with the electrolyte and become incorporated with the SEI before they can ripen to supercritical size [118].

11.3 Theoretical studies

The complicated interplay between the spontaneously formed SEI layer and the interfacial and thermodynamic properties of Li metal causes difficulties in deconvoluting and modeling the system. Ely et al. developed a unified theoretical framework for the early stages of heterogeneous Li electrodeposition [120]. The relationship between the deposit contact angle and critical nucleation overpotential was determined, and decreased kinetic critical nuclei radius and incubation time were both found to favor increased overpotentials. A comprehensive plot mapping the different regimes of nucleation and growth is given, identifying the conditions (embryo size and overpotential) for thermodynamically unfavorable Li growth, metastable Li growth, and stable monodisperse Li nuclei growth. Various computational studies have investigated the adsorption and formation of single-atom Li or small Li clusters on graphene surfaces in terms of their electronic structures and relevant energies [121–123]. Yakobson et al. calculated the Li nucleation barrier and critical cluster size for various lithiation states of graphene using density functional theory, suggesting that the significantly decreased nucleation barrier for increased Li concentrations on graphene could promote dendrite formation (Fig. 10(e)) [123].

12 Summary and perspective

We have summarized recent progress in nanoscale materials design for Li metal batteries, as well as the nanoscale understanding of Li nucleation and deposition. Nanotechnology has played an increasingly important role in this field, bringing many new insights to materials design. Especially in recent years, nanotechnology has been extensively applied to either stabilize the electrodes or improve safety. For electrodes, methodologies on interfacial engineering, homogenizing Li-ion flux, and designing stable "hosts" have been well established and shown to have great promise, while the nanoengineering of other battery components such as separators and current collectors has also attracted increasing attention.

However, these as-developed technologies remain far from satisfactory from a practical perspective. In order to obtain stable cycling, high average CEs of >99.8% are favorable to guarantee minimal excess Li required in the cell. Moreover, the CE is strongly correlated with deposition morphology, with high CEs correlating to more uniform Li deposition with less "dead" Li. Excellent SEI stability is necessary to achieve these goals. Two aspects must be emphasized in electrode design. On one hand, a stable volume must be maintained by the Li metal anode in order to afford a stable SEI. Otherwise, the dramatic interfacial fluctuation of tens of micrometers can easily fracture or even destroy the SEI. On the other hand, appropriate surface protection or modification is required to either protect the surface or regulate the Li surface tension.

In this scenario, designing a stable host for Li metal is essential and necessary. Ideally, a composite Li metal electrode with zero volume change during cycling is a good starting point. A 3D form of Li within the host is favorable in order to homogenize the Li-ion flux and improve the power output. However, 3D Li has significantly increased surface area, which in turn necessitates a good surface protection. We consider two possible strategies capable of providing sufficient surface protection. In one option, the conventional artificial SEI techniques can be applied to 3D Li to directly form a stable passivation layer. Alternatively, a nanoscale solid-state Li-ion conductive matrix can be generated as the host material, while metallic Li fills all the residual space within the matrix. In this case, a dense electrode with minimal surface exposure can be obtained, while the electrochemical activity of the large surface area of Li is simultaneously maintained by the Li-ion conductive network.

Understanding the nucleation and deposition behavior of Li at different stages of battery cycling under different chemical environments is also of great importance. It has been found that the nucleation and deposition behaviors can differ completely under

only slight variations in the composition of electrolytes. At present, a deep understanding of the correlations among nucleation and deposition behaviors, electrolyte compositions, surface tension, and SEI layers remains absent. However, understanding these relationships will be very helpful to guide the development of both new electrolytes or additives and artificial SEI layers. To achieve this goal, microscopic studies on the solid–liquid interface, assisted with electrochemical and spectroscopic analysis, would be indispensable.

Nanotechnology has become important in the development of Li metal batteries, and its importance will only increase in the future. Significant potential has been demonstrated by the various nanoscale approaches discussed in this review. The final success of the Li metal battery chemistry requires our continuous effort in both fundamental studies and materials development.

Acknowledgement

Y. C. acknowledges the support from the Assistant Secretary for Energy Efficiency and Renewable Energy, Office of Vehicle Technologies of the US Department of Energy under the Battery Materials Research Program and Battery500 Consortium.

References

[1] Tarascon, J.-M.; Armand, M. Issues and challenges facing rechargeable lithium batteries. *Nature* **2001**, *414*, 359–367.

[2] Chu, S.; Cui, Y.; Liu, N. The path towards sustainable energy. *Nat. Mater.* **2017**, *16*, 16–22.

[3] Xu, W.; Wang, J. L.; Ding, F.; Chen, X. L.; Nasybulin, E.; Zhang, Y. H.; Zhang, J.-G. Lithium metal anodes for rechargeable batteries. *Energy Environ. Sci.* **2014**, *7*, 513–537.

[4] Lin, D. C.; Liu, Y. Y.; Cui, Y. Reviving the lithium metal anode for high-energy batteries. *Nat. Nanotechnol.* **2017**, *12*, 194–206.

[5] Qian, J. F.; Henderson, W. A.; Xu, W.; Bhattacharya, P.; Engelhard, M.; Borodin, O.; Zhang, J.-G. High rate and stable cycling of lithium metal anode. *Nat. Commun.* **2015**, *6*, 6362.

[6] Qian, J. F.; Adams, B. D.; Zheng, J. M.; Xu, W.; Henderson, W. A.; Wang, J.; Bowden, M. E.; Xu, S. C.; Hu, J. Z.; Zhang, J. G. Anode-free rechargeable lithium metal batteries. *Adv. Funct. Mater.* **2016**, *26*, 7094–7102.

[7] Liu, B.; Xu, W.; Yan, P. F.; Sun, X. L.; Bowden, M. E.; Read, J.; Qian, J. F.; Mei, D. H.; Wang, C. M.; Zhang, J. G. Enhanced cycling stability of rechargeable Li–O_2 batteries using high-concentration electrolytes. *Adv. Funct. Mater.* **2016**, *26*, 605–613.

[8] Cao, R. G.; Chen, J. Z.; Han, K. S.; Xu, W.; Mei, D. H.; Bhattacharya, P.; Engelhard, M. H.; Mueller, K. T.; Liu, J.; Zhang, J.-G. Effect of the anion activity on the stability of Li metal anodes in lithium-sulfur batteries. *Adv. Funct. Mater.* **2016**, *26*, 3059–3066.

[9] Brandt, K. Historical development of secondary lithium batteries. *Solid State Ionics* **1994**, *69*, 173–183.

[10] Whittingham, M. S. Lithium batteries and cathode materials. *Chem. Rev.* **2004**, *104*, 4271–4302.

[11] Bruce, P. G.; Freunberger, S. A.; Hardwick, L. J.; Tarascon, J.-M. Li-O_2 and Li-S batteries with high energy storage. *Nat. Mater.* **2012**, *11*, 19–29.

[12] Xu, K. Electrolytes and interphases in Li-ion batteries and beyond. *Chem. Rev.* **2014**, *114*, 11503–11618.

[13] Zhang, R.; Li, N.-W.; Cheng, X.-B.; Yin, Y.-X.; Zhang, Q.; Guo, Y.-G. Advanced micro/nanostructures for lithium metal anodes. *Adv. Sci.* **2017**, *4*, 1600445.

[14] Peled, E. The electrochemical behavior of alkali and alkaline earth metals in nonaqueous battery systems—The solid electrolyte interphase model. *J. Electrochem. Soc.* **1979**, *126*, 2047–2051.

[15] Aurbach, D.; Daroux, M. L.; Faguy, P. W.; Yeager, E. Identification of surface films formed on lithium in propylene carbonate solutions. *J. Electrochem. Soc.* **1987**, *134*, 1611–1620.

[16] Peled, E.; Golodnitsky, D.; Ardel, G. Advanced model for solid electrolyte interphase electrodes in liquid and polymer electrolytes. *J. Electrochem. Soc.* **1997**, *144*, L208–L210.

[17] Aurbach, D. Review of selected electrode–solution interactions which determine the performance of Li and Li ion batteries. *J. Power Sources* **2000**, *89*, 206–218.

[18] Lin, D. C.; Liu, Y. Y.; Liang, Z.; Lee, H.-W.; Sun, J.; Wang, H. T.; Yan, K.; Xie, J.; Cui, Y. Layered reduced graphene oxide with nanoscale interlayer gaps as a stable host for lithium metal anodes. *Nat. Nanotechnol.* **2016**, *11*, 626–632.

[19] Lu, Y. Y.; Tu, Z. Y.; Archer, L. A. Stable lithium electrodeposition in liquid and nanoporous solid electrolytes. *Nat. Mater.* **2014**, *13*, 961–969.

[20] Liu, Q.-C.; Xu, J.-J.; Yuan, S.; Chang, Z.-W.; Xu, D.; Yin, Y.-B.; Li, L.; Zhong, H.-X.; Jiang, Y.-S.; Yan, J.-M. et al. Artificial protection film on lithium metal anode toward long-cycle-life lithium–oxygen batteries. *Adv. Mater.* **2015**, *27*, 5241–5247.

[21] Zhang, X.-Q.; Cheng, X.-B.; Chen, X.; Yan, C.; Zhang, Q. Fluoroethylene carbonate additives to render uniform Li deposits in lithium metal batteries. *Adv. Funct. Mater.* **2017**, *10*, 1605989.

[22] Lee, H.; Lee, D. J.; Kim, Y.-J.; Park, J.-K.; Kim, H.-T. A simple composite protective layer coating that enhances the cycling stability of lithium metal batteries. *J. Power Sources* **2015**, *284*, 103–108.

[23] Lee, D. J.; Lee, H.; Song, J.; Ryou, M.-H.; Lee, Y. M.; Kim, H.-T.; Park, J.-K. Composite protective layer for Li metal anode in high-performance lithium–oxygen batteries. *Electrochem. Commun.* **2014**, *40*, 45–48.

[24] Kozen, A. C.; Lin, C.-F.; Pearse, A. J.; Schroeder, M. A.; Han, X. G.; Hu, L. B.; Lee, S.-B.; Rubloff, G. W.; Noked, M. Next-generation lithium metal anode engineering via atomic layer deposition. *ACS Nano* **2015**, *9*, 5884–5892.

[25] Kazyak, E.; Wood, K. N.; Dasgupta, N. P. Improved cycle life and stability of lithium metal anodes through ultrathin atomic layer deposition surface treatments. *Chem. Mater.* **2015**, *27*, 6457–6462.

[26] Ma, G. Q.; Wen, Z. Y.; Wu, M. F.; Shen, C.; Wang, Q. S.; Jin, J.; Wu, X. W. A lithium anode protection guided highly-stable lithium–sulfur battery. *Chem. Commun.* **2014**, *50*, 14209–14212.

[27] Wu, M. F.; Wen, Z. Y.; Liu, Y.; Wang, X. Y.; Huang, L. Z. Electrochemical behaviors of a Li_3N modified Li metal electrode in secondary lithium batteries. *J. Power Sources* **2011**, *196*, 8091–8097.

[28] Li, N. W.; Yin, Y. X.; Yang, C. P.; Guo, Y. G. An artificial solid electrolyte interphase layer for stable lithium metal anodes. *Adv. Mater.* **2016**, *28*, 1853–1858.

[29] Wang, L. P.; Wang, Q. J.; Jia, W. S.; Chen, S. L.; Gao, P.; Li, J. Z. Li metal coated with amorphous Li_3PO_4 via magnetron sputtering for stable and long-cycle life lithium metal batteries. *J. Power Sources* **2017**, *342*, 175–182.

[30] Dudney, N. J. Addition of a thin-film inorganic solid electrolyte (Lipon) as a protective film in lithium batteries with a liquid electrolyte. *J. Power Sources* **2000**, *89*, 176–179.

[31] Cao, Y. Q.; Meng, X. B.; Elam, J. W. Atomic layer deposition of Li_xAl_yS solid-state electrolytes for stabilizing lithium-metal anodes. *ChemElectroChem* **2016**, *3*, 858–863.

[32] Belov, D. G.; Yarmolenko, O. V.; Peng, A.; Efimov, O. N. Lithium surface protection by polyacetylene *in situ* polymerization. *Synth. Metals* **2006**, *156*, 745–751.

[33] Choi, S. M.; Kang, I. S.; Sun, Y.-K.; Song, J.-H.; Chung, S.-M.; Kim, D.-W. Cycling characteristics of lithium metal batteries assembled with a surface modified lithium electrode. *J. Power Sources* **2013**, *244*, 363–368.

[34] Takehara, Z.-I.; Ogumi, Z.; Uchimoto, Y.; Yasuda, K.; Yoshida, H. Modification of lithium/electrolyte interface by plasma polymerization of 1,1-difluoroethene. *J. Power Sources* **1993**, *44*, 377–383.

[35] Jang, I. C.; Ida, S.; Ishihara, T. Surface coating layer on Li metal for increased cycle stability of Li–O_2 batteries. *J. Electrochem. Soc.* **2014**, *161*, A821–A826.

[36] Song, J.; Lee, H.; Choo, M.-J.; Park, J.-K.; Kim, H.-T. Ionomer-liquid electrolyte hybrid ionic conductor for high cycling stability of lithium metal electrodes. *Sci. Rep.* **2015**, *5*, 14458.

[37] Jin, Z. Q.; Xie, K.; Hong, X. B.; Hu, Z. Q.; Liu, X. Application of lithiated Nafion ionomer film as functional separator for lithium sulfur cells. *J. Power Sources* **2012**, *218*, 163–167.

[38] Lu, Y. Y.; Tikekar, M.; Mohanty, R.; Hendrickson, K.; Ma, L.; Archer, L. A. Stable cycling of lithium metal batteries using high transference number electrolytes. *Adv. Energy Mater.* **2015**, *5*, 1402073.

[39] Liu, Y. Y.; Lin, D. C.; Yuen, P. Y.; Liu, K.; Xie, J.; Dauskardt, R. H.; Cui, Y. An artificial solid electrolyte interphase with high Li-ion conductivity, mechanical strength, and flexibility for stable lithium metal anodes. *Adv. Mater.* **2017**, *10*, 1605531.

[40] Kim, J.-H.; Woo, H.-S.; Kim, W. K.; Ryu, K. H.; Kim, D.-W. Improved cycling performance of lithium–oxygen cells by use of a lithium electrode protected with conductive polymer and aluminum fluoride. *ACS Appl. Mater. Interfaces* **2016**, *8*, 32300–32306.

[41] Li, W. Y.; Yao, H. B.; Yan, K.; Zheng, G. Y.; Liang, Z.; Chiang, Y.-M.; Cui, Y. The synergetic effect of lithium polysulfide and lithium nitrate to prevent lithium dendrite growth. *Nat. Commun.* **2015**, *6*, 7436.

[42] Cheng, X.-B.; Yan, C.; Chen, X.; Guan, C.; Huang, J.-Q.; Peng, H.-J.; Zhang, R.; Yang, S.-T.; Zhang, Q. Implantable solid electrolyte interphase in lithium-metal batteries. *Chem* **2017**, *2*, 258–270.

[43] Zheng, G. Y.; Lee, S. W.; Liang, Z.; Lee, H.-W.; Yan, K.; Yao, H. B.; Wang, H. T.; Li, W. Y.; Chu, S.; Cui, Y. Interconnected hollow carbon nanospheres for stable lithium metal anodes. *Nat. Nanotechnol.* **2014**, *9*, 618–623.

[44] Yan, K.; Lee, H.-W.; Gao, T.; Zheng, G. Y.; Yao, H. B.; Wang, H. T.; Lu, Z. D.; Zhou, Y.; Liang, Z.; Liu, Z. F. et al. Ultrathin two-dimensional atomic crystals as stable interfacial layer for improvement of lithium metal anode. *Nano Lett.* **2014**, *14*, 6016–6022.

[45] Zhu, B.; Jin, Y.; Hu, X. Z.; Zheng, Q. H.; Zhang, S.; Wang, Q. J.; Zhu, J. Poly(dimethylsiloxane) thin film as a stable interfacial layer for high-performance lithium-metal battery anodes. *Adv. Mater.* **2017**, *29*, 1603755.

[46] Zheng, G. Y.; Wang, C.; Pei, A.; Lopez, J.; Shi, F. F.; Chen, Z.; Sendek, A. D.; Lee, H.-W.; Lu, Z. D.; Schneider, H. et al. High-performance lithium metal negative electrode with a soft and flowable polymer coating. *ACS Energy Lett.* **2016**, *1*, 1247–1255.

[47] Liu, W.; Li, W. Y.; Zhuo, D.; Zheng, G. Y.; Lu, Z. D.; Liu, K.; Cui, Y. Core–shell nanoparticle coating as an interfacial layer

for dendrite-free lithium metal anodes. *ACS Cent. Sci.* **2017**, *3*, 135–140.

[48] Yang, C.-P.; Yin, Y.-X.; Zhang, S.-F.; Li, N.-W.; Guo, Y.-G. Accommodating lithium into 3D current collectors with a submicron skeleton towards long-life lithium metal anodes. *Nat. Commun.* **2015**, *6*, 8058.

[49] Lu, L.-L.; Ge, J.; Yang, J.-N.; Chen, S.-M.; Yao, H. B.; Zhou, F.; Yu, S.-H. Free-standing copper nanowire network current collector for improving lithium anode performance. *Nano Lett.* **2016**, *16*, 4431–4437.

[50] Yun, Q. B.; He, Y. B.; Lv, W.; Zhao, Y.; Li, B. H.; Kang, F. Y.; Yang, Q. H. Chemical dealloying derived 3D porous current collector for Li metal anodes. *Adv. Mater.* **2016**, *28*, 6932–6939.

[51] Neuhold, S.; Schroeder, D. J.; Vaughey, J. T. Effect of surface preparation and R-group size on the stabilization of lithium metal anodes with silanes. *J. Power Sources* **2012**, *206*, 295–300.

[52] Wang, C.; Wang, D. L.; Dai, C. S. High-rate capability and enhanced cyclability of rechargeable lithium batteries using foam lithium anode. *J. Electrochem. Soc.* **2008**, *155*, A390–A394.

[53] Lee, H.; Song, J.; Kim, Y.-J.; Park, J.-K.; Kim, H.-T. Structural modulation of lithium metal-electrolyte interface with three-dimensional metallic interlayer for high-performance lithium metal batteries. *Sci. Rep.* **2016**, *6*, 30830.

[54] Ji, X. L.; Liu, D.-Y.; Prendiville, D. G.; Zhang, Y. C.; Liu, X. N.; Stucky, G. D. Spatially heterogeneous carbon-fiber papers as surface dendrite-free current collectors for lithium deposition. *Nano Today* **2012**, *7*, 10–20.

[55] Cheng, X.-B.; Peng, H.-J.; Huang, J.-Q.; Zhang, R.; Zhao, C.-Z.; Zhang, Q. Dual-phase lithium metal anode containing a polysulfide-induced solid electrolyte interphase and nanostructured graphene framework for lithium–sulfur batteries. *ACS Nano* **2015**, *9*, 6373–6382.

[56] Zhang, R.; Cheng, X.-B.; Zhao, C.-Z.; Peng, H.-J.; Shi, J.-L.; Huang, J.-Q.; Wang, J. F.; Wei, F.; Zhang, Q. Conductive nanostructured scaffolds render low local current density to inhibit lithium dendrite growth. *Adv. Mater.* **2016**, *28*, 2155–2162.

[57] Zhang, Y.; Liu, B. Y.; Hitz, E.; Luo, W.; Yao, Y. G.; Li, Y. J.; Dai, J. Q.; Chen, C. J.; Wang, Y. B.; Yang, C. P. et al. A carbon-based 3D current collector with surface protection for Li metal anode. *Nano Res.* **2017**, *10*, 1356–1365.

[58] Xie, K. Y.; Wei, W. F.; Yuan, K.; Lu, W.; Guo, M.; Li, Z. H.; Song, Q.; Liu, X. R.; Wang, J.-G.; Shen, C. Toward dendrite-free lithium deposition via structural and interfacial synergistic effects of 3D graphene@ Ni scaffold. *ACS Appl. Mater. Interfaces* **2016**, *8*, 26091–26097.

[59] Sun, Y. M.; Zheng, G. Y.; Seh, Z. W.; Liu, N.; Wang, S.; Sun, J.; Lee, H. R.; Cui, Y. Graphite-encapsulated Li-metal hybrid anodes for high-capacity Li batteries. *Chem* **2016**, *1*, 287–297.

[60] Ryou, M. H.; Lee, Y. M.; Lee, Y.; Winter, M.; Bieker, P. Mechanical surface modification of lithium metal: Towards improved Li metal anode performance by directed Li plating. *Adv. Funct. Mater.* **2015**, *25*, 834–841.

[61] Park, J.; Jeong, J.; Lee, Y.; Oh, M.; Ryou, M.-H.; Lee, Y. M. Micro-patterned lithium metal anodes with suppressed dendrite formation for post lithium-ion batteries. *Adv. Mater. Interfaces* **2016**, *3*, 1600140.

[62] Kim, J. S.; Yoon, W. Y. Improvement in lithium cycling efficiency by using lithium powder anode. *Electrochim. Acta* **2004**, *50*, 531–534.

[63] Hong, S.-T.; Kim, J.-S.; Lim, S.-J.; Yoon, W. Y. Surface characterization of emulsified lithium powder electrode. *Electrochim. Acta* **2004**, *50*, 535–539.

[64] Heine, J.; Krüger, S.; Hartnig, C.; Wietelmann, U.; Winter, M.; Bieker, P. Coated lithium powder (CLiP) electrodes for lithium-metal batteries. *Adv. Energy Mater.* **2014**, *4*, 1300815.

[65] Liang, Z.; Zheng, G. Y.; Liu, C.; Liu, N.; Li, W. Y.; Yan, K.; Yao, H. B.; Hsu, P.-C.; Chu, S.; Cui, Y. Polymer nanofiber-guided uniform lithium deposition for battery electrodes. *Nano Lett.* **2015**, *15*, 2910–2916.

[66] Cheng, X. B.; Hou, T. Z.; Zhang, R.; Peng, H. J.; Zhao, C. Z.; Huang, J. Q.; Zhang, Q. Dendrite-free lithium deposition induced by uniformly distributed lithium ions for efficient lithium metal batteries. *Adv. Mater.* **2016**, *28*, 2888–2895.

[67] Zhang, A. Y.; Fang, X.; Shen, C. F.; Liu, Y. H.; Zhou, C. W. A carbon nanofiber network for stable lithium metal anodes with high Coulombic efficiency and long cycle life. *Nano Res.* **2016**, *9*, 3428–3436.

[68] Zhang, D.; Zhou, Y.; Liu, C. H.; Fan, S. S. The effect of the carbon nanotube buffer layer on the performance of a Li metal battery. *Nanoscale* **2016**, *8*, 11161–11167.

[69] Zhang, D.; Yin, Y. L.; Liu, C. H.; Fan, S. S. Modified secondary lithium metal batteries with the polyaniline–carbon nanotube composite buffer layer. *Chem. Commun.* **2015**, *51*, 322–325.

[70] Xie, K. Y.; Yuan, K.; Zhang, K.; Shen, C.; Lv, W. B.; Liu, X. R.; Wang, J.-G.; Wei, B. Q. Dual functionalities of carbon nanotube films for dendrite-free and high energy–high power lithium–sulfur batteries. *ACS Appl. Mater. Interfaces* **2017**, *9*, 4605–4613.

[71] Liang, Z.; Lin, D. C.; Zhao, J.; Lu, Z. D.; Liu, Y. Y.; Liu, C.; Lu, Y. Y.; Wang, H. T.; Yan, K.; Tao, X. Y. et al. Composite lithium metal anode by melt infusion of lithium into a 3D conducting scaffold with lithiophilic coating. *Proc. Natl. Acad. Sci. USA* **2016**, *113*, 2862–2867.

[72] Liu, Y. Y.; Lin, D. C.; Liang, Z.; Zhao, J.; Yan, K.; Cui, Y.

Lithium-coated polymeric matrix as a minimum volume-change and dendrite-free lithium metal anode. *Nat. Commun.* **2016**, *7*, 10992.

[73] Liu, S. S.; Yang, J.; Yin, L. C.; Li, Z. M.; Wang, J. L.; Nuli, Y. Lithium-rich $Li_{2.6}BMg_{0.05}$ alloy as an alternative anode to metallic lithium for rechargeable lithium batteries. *Electrochim. Acta* **2011**, *56*, 8900–8905.

[74] Cheng, X. B.; Peng, H. J.; Huang, J. Q.; Wei, F.; Zhang, Q. Dendrite-free nanostructured anode: Entrapment of lithium in a 3D fibrous matrix for ultra-stable lithium–sulfur batteries. *Small* **2014**, *10*, 4257–4263.

[75] Wang, C. W.; Gong, Y. H.; Liu, B. Y.; Fu, K.; Yao, Y. G.; Hitz, E.; Li, Y. J.; Dai, J. Q.; Xu, S. M.; Luo, W. et al. Conformal, nanoscale ZnO surface modification of garnet-based solid-state electrolyte for lithium metal anodes. *Nano Lett.* **2017**, *17*, 565–571.

[76] Luo, W.; Gong, Y. H.; Zhu, Y. Z.; Fu, K. K.; Dai, J. Q.; Lacey, S. D.; Wang, C. W.; Liu, B. Y.; Han, X. G.; Mo, Y. F. et al. Transition from superlithiophobicity to superlithiophilicity of garnet solid-state electrolyte. *J. Am. Chem. Soc.* **2016**, *138*, 12258–12262.

[77] Han, X. G.; Gong, Y. H.; Fu, K.; He, X. F.; Hitz, G. T.; Dai, J. Q.; Pearse, A.; Liu, B. Y.; Wang, H.; Rubloff, G. et al. Negating interfacial impedance in garnet-based solid-state Li metal batteries. *Nat. Mater.*, in press, DOI: 10.1038/nmat4821.

[78] Yan, K.; Lu, Z. D.; Lee, H.-W.; Xiong, F.; Hsu, P.-C.; Li, Y. Z.; Zhao, J.; Chu, S.; Cui, Y. Selective deposition and stable encapsulation of lithium through heterogeneous seeded growth. *Nat. Energy* **2016**, *1*, 16010.

[79] Kang, H.-K.; Woo, S.-G.; Kim, J.-H.; Yu, J.-S.; Lee, S.-R.; Kim, Y.-J. Few-layer graphene island seeding for dendrite-free Li metal electrodes. *ACS Appl. Mater. Interfaces* **2016**, *8*, 26895–26901.

[80] Ding, F.; Xu, W.; Graff, G. L.; Zhang, J.; Sushko, M. L.; Chen, X. L.; Shao, Y. Y.; Engelhard, M. H.; Nie, Z. M.; Xiao, J. et al. Dendrite-free lithium deposition via self-healing electrostatic shield mechanism. *J. Am. Chem. Soc.* **2013**, *135*, 4450–4456.

[81] Monroe, C.; Newman, J. Dendrite growth in lithium/polymer systems: A propagation model for liquid electrolytes under galvanostatic conditions. *J. Electrochem. Soc.* **2003**, *150*, A1377–A1384.

[82] Liu, W.; Lin, D. C.; Pei, A.; Cui, Y. Stabilizing lithium metal anodes by uniform Li-ion flux distribution in nanochannel confinement. *J. Am. Chem. Soc.* **2016**, *138*, 15443–15450.

[83] Kim, J.-H.; Kang, H.-K.; Woo, S.-G.; Jeong, G.; Park, M.-S.; Kim, K. J.; Yu, J.-S.; Yim, T.; Jo, Y. N.; Kim, H. et al. Oriented TiO_2 nanotubes as a lithium metal storage medium. *J. Electroanalyt. Chem.* **2014**, *726*, 51–54.

[84] Han, J.-H.; Khoo, E.; Bai, P.; Bazant, M. Z. Over-limiting current and control of dendritic growth by surface conduction in nanopores. *Sci. Rep.* **2014**, *4*, 7056.

[85] Bai, P.; Li, J.; Brushett, F. R.; Bazant, M. Z. Transition of lithium growth mechanisms in liquid electrolytes. *Energy Environ. Sci.* **2016**, *9*, 3221–3229.

[86] Kang, S. J.; Mori, T.; Suk, J.; Kim, D. W.; Kang, Y.; Wilcke, W.; Kim, H.-C. Improved cycle efficiency of lithium metal electrodes in Li–O_2 batteries by a two-dimensionally ordered nanoporous separator. *J. Mater. Chem. A* **2014**, *2*, 9970–9974.

[87] Arora, P.; Zhang, Z. M. Battery separators. *Chem. Rev.* **2004**, *104*, 4419–4462.

[88] Ryou, M. H.; Lee, D. J.; Lee, J. N.; Lee, Y. M.; Park, J. K.; Choi, J. W. Excellent cycle life of lithium-metal anodes in lithium-ion batteries with mussel-inspired polydopamine-coated separators. *Adv. Energy Mater.* **2012**, *2*, 645–650.

[89] Shi, C.; Dai, J. H.; Shen, X.; Peng, L. Q.; Li, C.; Wang, X.; Zhang, P.; Zhao, J. B. A high-temperature stable ceramic-coated separator prepared with polyimide binder/Al_2O_3 particles for lithium-ion batteries. *J. Membrane Sci.* **2016**, *517*, 91–99.

[90] Jeon, H.; Jin, S. Y.; Park, W. H.; Lee, H.; Kim, H.-T.; Ryou, M.-H.; Lee, Y. M. Plasma-assisted water-based Al_2O_3 ceramic coating for polyethylene-based microporous separators for lithium metal secondary batteries. *Electrochim. Acta* **2016**, *212*, 649–656.

[91] Kumar, J.; Kichambare, P.; Rai, A. K.; Bhattacharya, R.; Rodrigues, S.; Subramanyam, G. A high performance ceramic-polymer separator for lithium batteries. *J. Power Sources* **2016**, *301*, 194–198.

[92] Chi, M. M.; Shi, L. Y.; Wang, Z. Y.; Zhu, J. F.; Mao, X. F.; Zhao, Y.; Zhang, M. H.; Sun, L. N.; Yuan, S. Excellent rate capability and cycle life of Li metal batteries with ZrO_2/POSS multilayer-assembled PE separators. *Nano Energy* **2016**, *28*, 1–11.

[93] Jiang, W.; Liu, Z. H.; Kong, Q. S.; Yao, J. H.; Zhang, C. J.; Han, P. X.; Cui, G. L. A high temperature operating nanofibrous polyimide separator in Li-ion battery. *Solid State Ionics* **2013**, *232*, 44–48.

[94] Lin, D. C.; Zhuo, D.; Liu, Y. Y.; Cui, Y. All-integrated bifunctional separator for Li dendrite detection via novel solution synthesis of a thermostable polyimide separator. *J. Am. Chem. Soc.* **2016**, *138*, 11044–11050.

[95] Yu, B.-C.; Park, K.; Jang, J.-H.; Goodenough, J. B. Cellulose-based porous membrane for suppressing Li dendrite formation in lithium–sulfur battery. *ACS Energy Lett.* **2016**, *1*, 633–637.

[96] Chang, C.-H.; Chung, S.-H.; Manthiram, A. Dendrite-free lithium anode via a homogenous Li-ion distribution enabled by a kimwipe paper. *Adv. Sustainable Syst.* **2017**, *1*, 1600034.

[97] Tikekar, M. D.; Choudhury, S.; Tu, Z. Y.; Archer, L. A. Design principles for electrolytes and interfaces for stable lithium-metal batteries. *Nat. Energy* **2016**, *1*, 16114.

[98] Tikekar, M. D.; Archer, L. A.; Koch, D. L. Stabilizing electrodeposition in elastic solid electrolytes containing immobilized anions. *Sci. Adv.* **2016**, *2*, e1600320.

[99] Liu, K.; Bai, P.; Bazant, M. Z.; Wang, C.-A.; Li, J. A soft non-porous separator and its effectiveness in stabilizing Li metal anodes cycling at 10 $mA \cdot cm^{-2}$ observed *in situ* in a capillary cell. *J. Mater. Chem. A* **2017**, *5*, 4300–4307.

[100] Shin, W.-K.; Kannan, A. G.; Kim, D.-W. Effective suppression of dendritic lithium growth using an ultrathin coating of nitrogen and sulfur codoped graphene nanosheets on polymer separator for lithium metal batteries. *ACS Appl. Mater. Interfaces* **2015**, *7*, 23700–23707.

[101] Tung, S.-O.; Ho, S.; Yang, M.; Zhang, R. L.; Kotov, N. A. A dendrite-suppressing composite ion conductor from aramid nanofibres. *Nat. Commun.* **2015**, *6*, 6152.

[102] Hao, X. M.; Zhu, J.; Jiang, X.; Wu, H. T.; Qiao, J. S.; Sun, W.; Wang, Z. H.; Sun, K. N. Ultrastrong polyoxyzole nanofiber membranes for dendrite-proof and heat-resistant battery separators. *Nano Lett.* **2016**, *16*, 2981–2987.

[103] Monroe, C.; Newman, J. The impact of elastic deformation on deposition kinetics at lithium/polymer interfaces. *J. Electrochem. Soc.* **2005**, *152*, A396–A404.

[104] Ferrese, A.; Newman, J. Mechanical deformation of a lithium-metal anode due to a very stiff separator. *J. Electrochem. Soc.* **2014**, *161*, A1350–A1359.

[105] Wu, H.; Zhuo, D.; Kong, D. S.; Cui, Y. Improving battery safety by early detection of internal shorting with a bifunctional separator. *Nat. Commun.* **2014**, *5*, 5193.

[106] Liu, K.; Zhuo, D.; Lee, H. W.; Liu, W.; Lin, D. C.; Lu, Y. Y.; Cui, Y. Extending the life of lithium-based rechargeable batteries by reaction of lithium dendrites with a novel silica nanoparticle sandwiched separator. *Adv. Mater.* **2017**, *29*, 1603987.

[107] Chen, Z.; Hsu, P.-C.; Lopez, J.; Li, Y. Z.; To, J. W. F.; Liu, N.; Wang, C.; Andrews, S. C.; Liu, J.; Cui, Y. et al. Fast and reversible thermoresponsive polymer switching materials for safer batteries. *Nat. Energy* **2016**, *1*, 15009.

[108] Yim, T.; Park, M.-S.; Woo, S.-G.; Kwon, H.-K.; Yoo, J.-K.; Jung, Y. S.; Kim, K. J.; Yu, J.-S.; Kim, Y.-J. Self-extinguishing lithium ion batteries based on internally embedded fire-extinguishing microcapsules with temperature-responsiveness. *Nano Lett.* **2015**, *15*, 5059–5067.

[109] Liu, K.; Liu, W.; Qiu, Y. C.; Kong, B.; Sun, Y. M.; Chen, Z.; Zhuo, D.; Lin, D. C.; Cui, Y. Electrospun core–shell microfiber separator with thermal-triggered flame-retardant properties for lithium-ion batteries. *Sci. Adv.* **2017**, *3*, e1601978.

[110] Aurbach, D.; Zinigrad, E.; Cohen, Y.; Teller, H. A short review of failure mechanisms of lithium metal and lithiated graphite anodes in liquid electrolyte solutions. *Solid State Ionics* **2002**, *148*, 405–416.

[111] Steiger, J. Mechanisms of dendrite growth in lithium metal batteries. Ph.D. Dissertation, Karlsruher Institut für Technologie (KIT), Karlsruhe, 2015.

[112] Yoo, S.-H.; Lee, J.-H.; Jung, Y.-K.; Soon, A. Exploring stereographic surface energy maps of cubic metals via an effective pair-potential approach. *Phys. Rev. B* **2016**, *93*, 035434.

[113] Liu, Z. X.; Bertolini, S.; Balbuena, P. B.; Mukherjee, P. P. Li_2S film formation on lithium anode surface of Li–S batteries. *ACS App. Mater. Interfaces* **2016**, *8*, 4700–4708.

[114] Milchev, A. *Electrocrystallization: Fundamentals of Nucleation and Growth*; Springer: New York, 2002.

[115] Milchev, A.; Irene Montenegro, M. A galvanostatic study of electrochemical nucleation. *J. Electroanalyt. Chem.* **1992**, *333*, 93–102.

[116] Sano, H.; Sakaebe, H.; Senoh, H.; Matsumoto, H. Effect of current density on morphology of lithium electrodeposited in ionic liquid-based electrolytes. *J. Electrochem. Soc.* **2014**, *161*, A1236–A1240.

[117] Sagane, F.; Ikeda, K.-I.; Okita, K.; Sano, H.; Sakaebe, H.; Iriyama, Y. Effects of current densities on the lithium plating morphology at a lithium phosphorus oxynitride glass electrolyte/copper thin film interface. *J. Power Sources* **2013**, *233*, 34–42.

[118] Pei, A.; Zheng, G. Y.; Shi, F. F.; Li, Y. Z.; Cui, Y. Nanoscale nucleation and growth of electrodeposited lithium metal. *Nano Lett.* **2017**, *17*, 1132–1139.

[119] Stark, J. K.; Ding, Y.; Kohl, P. A. Nucleation of electro-deposited lithium metal: Dendritic growth and the effect of co-deposited sodium. *J. Electrochem. Soc.* **2013**, *160*, D337–D342.

[120] Ely, D. R.; García, R. E. Heterogeneous nucleation and growth of lithium electrodeposits on negative electrodes. *J. Electrochem. Soc.* **2013**, *160*, A662–A668.

[121] Garay-Tapia, A. M.; Romero, A. H.; Barone, V. Lithium adsorption on graphene: From isolated adatoms to metallic sheets. *J. Chem. Theory Comput.* **2012**, *8*, 1064–1071.

[122] Fan, X. F.; Zheng, W. T.; Kuo, J.-L.; Singh, D. J. Adsorption of single Li and the formation of small Li clusters on graphene for the anode of lithium-ion batteries. *ACS Appl. Mater. Interfaces* **2013**, *5*, 7793–7797.

[123] Liu, M. J.; Kutana, A.; Liu, Y. Y.; Yakobson, B. I. First-principles studies of Li nucleation on graphene. *J. Phys. Chem. Lett.* **2014**, *5*, 1225–1229.